

Dynamics of warped accretion discs

Scott Tremaine^{1*}, Shane W. Davis^{2†}

¹*Institute for Advanced Study, Princeton, NJ 08540, USA*

²*Canadian Institute for Theoretical Astrophysics, University of Toronto, Toronto, ON M5S 3H8, Canada*

30 October 2018

ABSTRACT

Accretion discs are present around both stellar-mass black holes in X-ray binaries and supermassive black holes in active galactic nuclei. A wide variety of circumstantial evidence implies that many of these discs are warped. The standard Bardeen–Petterson model attributes the shape of the warp to the competition between Lense–Thirring torque from the central black hole and viscous angular-momentum transport within the disc. We show that this description is incomplete, and that torques from the companion star (for X-ray binaries) or the self-gravity of the disc (for active galactic nuclei) can play a major role in determining the properties of the warped disc. Including these effects leads to a rich set of new phenomena. For example, (i) when a companion star is present and the warp arises from a misalignment between the companion’s orbital axis and the black hole’s spin axis, there is no steady-state solution of the Pringle–Ogilvie equations for a thin warped disc when the viscosity falls below a critical value; (ii) in AGN accretion discs, the warp can excite short-wavelength bending waves that propagate inward with growing amplitude until they are damped by the disc viscosity. We show that both phenomena can occur for plausible values of the black hole and disc parameters, and briefly discuss their observational implications.

Key words: accretion, accretion discs – black hole physics – hydrodynamics – binaries: close – X-rays: binaries – galaxies: active

1 INTRODUCTION

The study of warped discs dates back to Laplace’s (1805) study of the motions of the satellites of Jupiter, in which he showed that each satellite precessed around an axis on which the orbit-averaged torques from the quadrupole moment of the planet and the tidal field from the Sun cancelled. The locus of the circular rings defined by these axes, now called the Laplace surface, is the expected shape of a dissipative low-viscosity disc in this potential (for a review see Tremaine et al. 2009).

More recent studies of warped accretion discs began with Bardeen & Petterson (1975), who pointed out that an accretion disc orbiting a spinning black hole (BH) would be subject to Lense–Thirring torque if its orbital axis were not aligned with the spin axis of the BH; this torque leads to precession of the axis of a test particle on a circular orbit of radius r at an angular speed $\omega = 2G\mathbf{L}_\bullet/(r^3c^2)$, where \mathbf{L}_\bullet is the angular momentum of the BH¹.

We call discs ‘quadrupole’ or ‘Lense–Thirring’ discs depending on which determines the torque from the central body. There are fundamental differences in the behavior of warped quadrupole and Lense–Thirring discs. The first is that if the spin axis of the central body is reversed, the Lense–Thirring torque is also reversed (eq. 3) but the quadrupole torque is not (eq. 2). A second and more fundamental difference is the sign of the torque: for small inclinations the quadrupole torque induces retrograde precession of the angular momentum of the disc around the spin axis of the central body, whereas the Lense–Thirring torque induces prograde precession. The shape of a steady-state warped disc is determined by the requirement that the sum of the torques from all external sources equals the divergence of the angular-momentum currents from transport

* E-mail: tremaine@ias.edu

† E-mail: swd@cita.utoronto.ca

¹ The quadrupole moment of the BH also leads to precession, but this is usually less important as its effects fall off faster with radius by a factor $r^{-1/2}$.

within the disc (eqs. 23–25); thus the difference in sign of the quadrupole and Lense–Thirring torque leads to fundamental differences in the geometry of the corresponding discs (§1.2).

Warps are also categorized as ‘small-amplitude’ or ‘large-amplitude’ depending on whether the amplitude of the warp is smaller or larger than the disc thickness. The first self-consistent equations governing warps in viscous fluid discs were derived by Papaloizou & Pringle (1983) in the small-amplitude approximation; their treatment assumed (as we do in this paper) that the equation of state is barotropic, that the disc material at radius r is azimuthally symmetric about some symmetry axis $\hat{\mathbf{n}}(r)$ parallel to the local angular-momentum vector, that the disc is thin ($H/r \ll 1$), and that the time evolution of the disc is slow ($\partial/\partial t \ll \Omega$ where $\Omega^2 = GM/r^3$ is the squared angular speed of a Keplerian ring). Among other results Papaloizou & Pringle (1983) found that the behavior of near-Keplerian discs is complicated by a global resonance between the azimuthal and radial frequencies Ω and κ of test particles in a Keplerian potential. Non-resonant behavior requires that

$$\alpha \quad \text{or} \quad |1 - \kappa^2/\Omega^2| \gtrsim H/r \quad (1)$$

where α is the dimensionless Shakura–Sunyaev (1973) viscosity parameter (eq. 26). Most astrophysical discs are non-resonant in this sense, and we shall assume that this is so in our analysis. An additional complication, which we shall ignore, is that the strong, oscillating, shearing flows generated by this near-resonance are likely to be unstable to the development of turbulence (see Ogilvie & Latter 2013b, and references therein), especially for the low viscosities and large warps that occupy much of our discussion.

The equations governing the viscous evolution of thin discs with large-amplitude warps were derived by Pringle (1992) and Ogilvie (1999); a simplified local derivation of the equations is given by Ogilvie & Latter (2013a). These authors point out that the evolution of a twisted disc depends on three conceptually distinct transport coefficients: ν_1 is the usual viscosity associated with flat accretion discs, which produces a torque parallel to the local disc normal² $\hat{\mathbf{n}}(r)$ that tends to bring adjacent rings to the same angular speed; ν_2 is associated with the shear normal to the disc and produces a torque proportional to $\partial\hat{\mathbf{n}}/\partial r$ that tends to bring adjacent rings to the same orientation; and ν_3 produces a torque that is proportional to $\hat{\mathbf{n}} \times \partial\hat{\mathbf{n}}/\partial r$ and advects angular momentum in a warped disc. In general these three transport coefficients are not equal, and a specific model for the stress tensor in the disc fluid is required to determine their values. Ogilvie (1999) carries out this determination for Shakura–Sunyaev discs, in which the shear and bulk viscosity are given by equation (26); see for example Fig. 2. However, it is unclear how directly this treatment applies to real discs, where the stress tensor is thought to be determined by magnetohydrodynamic (MHD) turbulence (see §2.1).

The evolution and steady-state shape of warped accretion discs can be determined by a variety of competing effects: the quadrupole or Lense–Thirring torque from the central body; mass and angular-momentum transport through the disc due to viscosity; the tidal field from a companion object (the Sun for planetary satellites or a stellar companion for X-ray binary stars); the self-gravity of the disc; radiation pressure from the central object; magnetic fields; etc. We shall not consider radiation pressure (Pringle 1996) or magnetic fields (Lai 1999) in this paper, although some of the phenomena that we describe have analogs when these effects are important. We distinguish ‘high-viscosity’ from ‘low-viscosity’ discs depending on whether the torque associated with viscous angular-momentum transport plays a dominant role in determining the shape of the warped disc (see §1.3).

What we mean by the self-gravity of the disc needs to be amplified. There are different ways in which discs can be ‘self-gravitating’. (i) The radial gravitational force from the disc can be comparable to the gravity from the host BH, which requires that the surface density $\Sigma \gtrsim M/r^2$; this case is not relevant for most accretion discs and we shall not discuss it further. (ii) Within the disc, the vertical gravitational force from the disc can be comparable to the vertical gravity from the BH; this requires that the density in the disc is of order M/r^3 or that Toomre’s (1964) Q parameter (eq. 69) is of order unity. Models of accretion discs with $Q \simeq 1$ were first described by Paczyński (1978); in accretion discs surrounding supermassive BHs in active galactic nuclei (AGN) this condition is likely to be satisfied at distances exceeding ~ 0.01 pc, and such discs may fragment into stars (Goodman 2003). (iii) The apsidal and/or nodal precession rate of the disc may be dominated by self-gravity; for AGN accretion discs this requires far less mass than cases (i) or (ii) and this is the case that we focus on here.

Remarkably, almost all previous studies of warped Lense–Thirring discs follow Bardeen and Petterson in considering only torques from the central body and viscous torques in their analyses. We shall show that the other two effects listed in the preceding paragraph – gravitational torques from the companion and the self-gravity of the disc – can introduce qualitatively new phenomena in the behavior of warped discs surrounding stellar-mass and supermassive BHs, respectively. In particular, (i) warped low-viscosity discs exhibit a sharp depression in their surface density near the radius where the warp is strongest; (ii) steady-state Lense–Thirring discs do not exist, at least within the standard thin disc description, for viscosities below a critical value that depends on the obliquity (the angle between the BH spin angular momentum and the companion orbital angular momentum); (iii) warped low-viscosity discs in which self-gravity is important can develop strong short-wavelength bending waves.

² Note that $\hat{\mathbf{n}}(r)$ is the normal to the orbital plane of the ring at radius r but not the normal to the disc surface at radius r , which in general depends on azimuth.

As a preliminary step, §§1.1 and 1.2 derive the steady-state properties of warped discs in which viscosity is negligible. Then §1.3 provides a broad-brush overview of the competing effects that determine the behavior of warped discs. Section 2.1 derives the equations of motion for a thin, viscous disc subjected to external torques, following Pringle (1992) and Ogilvie (1999), and §2.3 describes our numerical methods and the results for both quadrupole and Lense–Thirring discs in systems with a binary companion. Section 3 describes the behavior of self-gravitating warped discs. Section 4 relates our findings to earlier work on warped accretion discs. Sections 5.1 and 5.2 apply our results to accretion discs around stellar-mass BHs in binary systems, around supermassive black holes in AGN. Finally, §6 contains a brief summary of our conclusions.

1.1 External torques

In this paper we consider three types of external torque that can warp an accretion disc. In each case we shall assume that the torque is weak – the fractional change per orbit in the angular momentum of an orbiting fluid element is small – so we can work with the orbit-averaged torque. In particular we define $\mathbf{T}(r, \hat{\mathbf{n}}, t)$ to be the torque per unit mass averaged over a circular orbit at radius r with orbit normal $\hat{\mathbf{n}}$.

Quadrupole torque: In the system examined by Laplace, the central body is a planet of mass M , radius R_p , and quadrupole gravitational harmonic J_2 . If the planet’s spin axis is along $\hat{\mathbf{n}}_p$, the torque per unit mass on an orbiting test particle is

$$\mathbf{T}_p = \frac{\epsilon_p}{r^3} (\hat{\mathbf{n}} \cdot \hat{\mathbf{n}}_p) \hat{\mathbf{n}} \times \hat{\mathbf{n}}_p \quad \text{where} \quad \epsilon_p = \frac{3}{2} GM J_2 R_p^2. \quad (2)$$

The quadrupole torque is also relevant to circumbinary accretion discs; in the case of a binary with masses M_1 and M_2 on a circular orbit with separation $a \ll r$, we replace M by $M_1 + M_2$ and $J_2 R_p^2$ by $\frac{1}{2} M_1 M_2 a^2 / (M_1 + M_2)^2$.

Lense–Thirring torque: The central body can also be a BH of mass M and angular momentum $\mathbf{L}_\bullet = GM^2 a_\bullet \hat{\mathbf{n}}_\bullet / c$ where c is the speed of light, $\hat{\mathbf{n}}_\bullet$ is the spin axis of the BH and $0 \leq a_\bullet < 1$ is the dimensionless spin parameter of the BH. The angular momentum of a test particle orbiting the BH precesses as if it were subject to a classical torque (the Lense–Thirring torque; see Landau & Lifshitz 2007)

$$\mathbf{T}_{\text{LT}} = -\frac{\epsilon_{\text{LT}}}{r^{5/2}} \hat{\mathbf{n}} \times \hat{\mathbf{n}}_\bullet \quad \text{where} \quad \epsilon_{\text{LT}} = \frac{2(GM)^{5/2} a_\bullet}{c^3} = 2R_g^{5/2} c^2 a_\bullet, \quad (3)$$

where $R_g \equiv GM/c^2 \ll r$ is the gravitational radius of the BH.

Companion torque The central body, whether a planet or a BH, may be accompanied by a companion star of mass M_\star , on a circular orbit with radius $r_\star \gg r$. Then the gravitational potential of the companion can be approximated by its quadrupole component, which after averaging over the companion orbit yields a torque

$$\mathbf{T}_\star = \epsilon_\star r^2 (\hat{\mathbf{n}} \cdot \hat{\mathbf{n}}_\star) \hat{\mathbf{n}} \times \hat{\mathbf{n}}_\star \quad \text{where} \quad \epsilon_\star = \frac{3GM_\star}{4r_\star^3}. \quad (4)$$

1.2 Inviscid discs

Following Laplace, we first consider a thin disc of material orbiting a planet with non-zero obliquity (the obliquity is $\cos^{-1} \hat{\mathbf{n}}_p \cdot \hat{\mathbf{n}}_\star$). The disc is subject to torques from the quadrupole moment of the planet, \mathbf{T}_p (eq. 2), and from the companion star around which the planet orbits, \mathbf{T}_\star (eq. 4). In the absence of pressure, viscosity, self-gravity, or other collective effects in the disc, the fluid rings at different radii precess independently, so the disc cannot retain its coherence unless the total torque $\mathbf{T}_\star + \mathbf{T}_p = 0$ at each radius. This requires

$$r^5 (\hat{\mathbf{n}} \cdot \hat{\mathbf{n}}_\star) \hat{\mathbf{n}} \times \hat{\mathbf{n}}_\star + \frac{\epsilon_p}{\epsilon_\star} (\hat{\mathbf{n}} \cdot \hat{\mathbf{n}}_p) \hat{\mathbf{n}} \times \hat{\mathbf{n}}_p = 0, \quad (5)$$

which can be rewritten as

$$\left(\frac{r}{r_w}\right)^5 (\hat{\mathbf{n}} \cdot \hat{\mathbf{n}}_\star) \hat{\mathbf{n}} \times \hat{\mathbf{n}}_\star + (\hat{\mathbf{n}} \cdot \hat{\mathbf{n}}_p) \hat{\mathbf{n}} \times \hat{\mathbf{n}}_p = 0 \quad \text{where} \quad r_w^5 \equiv \frac{\epsilon_p}{\epsilon_\star} = 2J_2 \frac{M}{M_\star} R_p^2 r_\star^3 \quad (6)$$

defines the characteristic radius r_w at which the warp is most prominent (Goldreich 1966).

We restrict ourselves to the usual case in which the disc normal $\hat{\mathbf{n}}(r)$ is coplanar with $\hat{\mathbf{n}}_p$ and $\hat{\mathbf{n}}_\star$ (for a more general discussion see Tremaine et al. 2009). Then the unit vectors $\hat{\mathbf{n}}(r)$, $\hat{\mathbf{n}}_p$, $\hat{\mathbf{n}}_\star$ can be specified by their azimuthal angles in this plane, $\phi(r)$, ϕ_p , ϕ_\star . Without loss of generality we may assume $\phi_\star = \frac{1}{2}\pi$, so the obliquity is $\phi_p - \phi_\star = \phi_p - \frac{1}{2}\pi$. Then equation (6) can be rewritten as

$$\left(\frac{r}{r_w}\right)^5 = \frac{\sin 2(\phi - \phi_p)}{\sin 2\phi}. \quad (7)$$

The solutions to equation (7) are shown in the left panel of Fig. 1 for obliquity $\phi_p - \phi_\star = 60^\circ$. The ‘classical’ Laplace

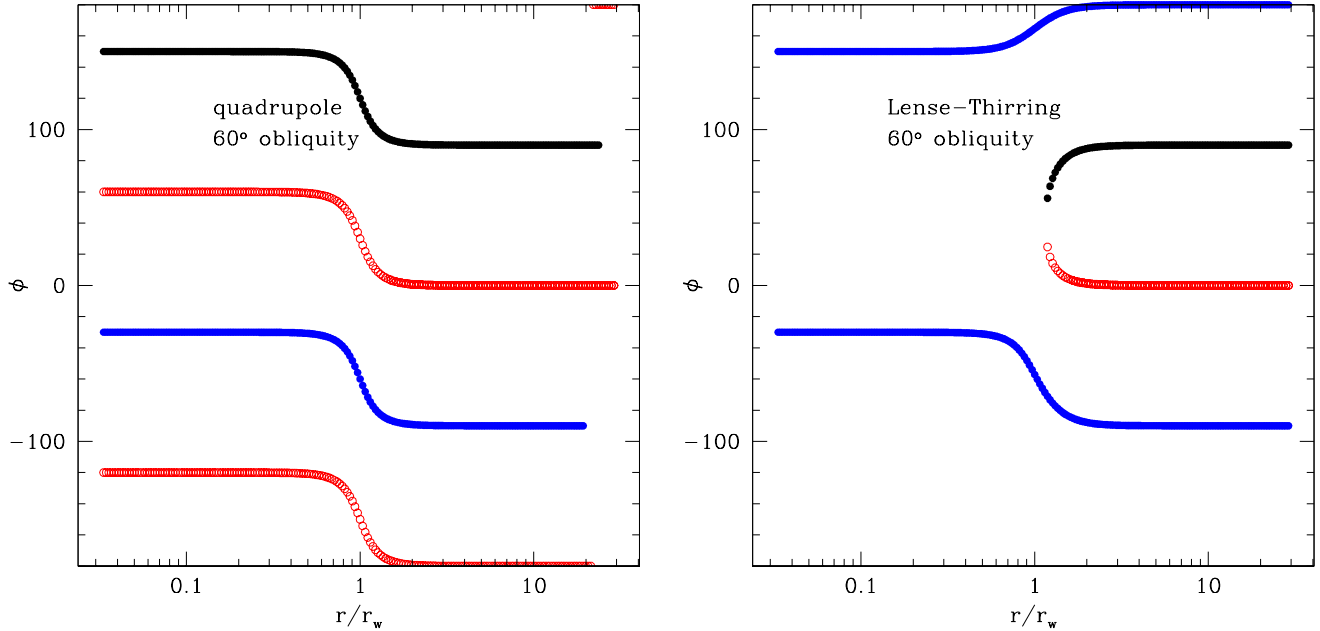


Figure 1. (left) The orientation of a stationary, inviscid disc orbiting a planet that has an obliquity of 60° . An orbit with angular momentum aligned with the planetary orbit has azimuthal angle $\phi = 90^\circ$ and an orbit aligned with the planetary equator has $\phi = 90^\circ + 60^\circ = 150^\circ$. The black solid circles denote the classical Laplace surface, the blue circles denote the same spatial surface as traced by retrograde orbits, and the red open circles denote dynamically unstable surfaces. (right) The same as the left panel, but for an inviscid disc orbiting a spinning BH; like the planet, the BH orbits a companion star with an obliquity of 60° .

surface, shown as solid black circles, is aligned with the planet’s orbit around the star at large radii ($\phi \rightarrow \frac{1}{2}\pi$ as $r \rightarrow \infty$). The surface shown by solid blue circles is similar, but composed of retrograde orbits (the disc angular-momentum vector is anti-aligned with the planetary orbital angular momentum at large radii, and anti-aligned with the planetary spin at small radii). The surfaces shown by open red circles are also solutions of equation (7) but they are unstable to small perturbations in $\hat{\mathbf{n}}$ (Tremaine et al. 2009), and we will not consider them further. On the classical Laplace surface, the azimuth of the disc normal ϕ increases smoothly and continuously from ϕ_* to ϕ_p , so that the disc plane gradually twists from the orbital plane of the planet to the equatorial plane of the planet as its radius shrinks.

We next carry out the analogous derivation for an inviscid thin disc orbiting a spinning BH with a companion star. The disc is subject to Lense–Thirring torque, \mathbf{T}_{LT} (eq. 3), and torque from the companion star, \mathbf{T}_* (eq. 4). The equilibrium shape defined by $\mathbf{T}_* + \mathbf{T}_{\text{LT}} = 0$ is given by

$$r^{9/2}(\hat{\mathbf{n}} \cdot \hat{\mathbf{n}}_*) \hat{\mathbf{n}} \times \hat{\mathbf{n}}_* - \frac{\epsilon_{\text{LT}}}{\epsilon_*} \hat{\mathbf{n}} \times \hat{\mathbf{n}}_\bullet = 0 \quad (8)$$

which can be rewritten as

$$\left(\frac{r}{r_w}\right)^{9/2} (\hat{\mathbf{n}} \cdot \hat{\mathbf{n}}_*) \hat{\mathbf{n}} \times \hat{\mathbf{n}}_* - \hat{\mathbf{n}} \times \hat{\mathbf{n}}_\bullet = 0 \quad \text{where} \quad r_w^{9/2} = \frac{\epsilon_{\text{LT}}}{\epsilon_*} = \frac{8a_\bullet}{3} \frac{M}{M_*} R_g^{3/2} r_*^3. \quad (9)$$

The analog to equation (7) is

$$\left(\frac{r}{r_w}\right)^{9/2} = -\frac{2 \sin(\phi - \phi_\bullet)}{\sin 2\phi}, \quad (10)$$

where ϕ_\bullet is the azimuthal angle of the BH spin axis. The obliquity is $\phi_\bullet - \phi_* = \phi_\bullet - \frac{1}{2}\pi$.

The solutions to equation (10) are shown in the right panel of Fig. 1 for obliquity $\phi_\bullet - \phi_* = 60^\circ$. In contrast to the quadrupole case, the solution that is aligned with the companion-star orbit at large radii ($\phi \rightarrow \frac{1}{2}\pi$ as $r \rightarrow \infty$, shown as black filled circles) terminates just outside the characteristic radius r_w (this solution is mirrored by an unstable solution, shown by open red circles, that has no relevance to our discussion). The solution that is aligned with the equator of the BH at small radii, shown as the upper set of filled blue circles, approaches $\phi = \pi$ at large radii; in other words the disc is perpendicular to the companion-star orbital plane, which is inconsistent with the expectation that the disc is fed by material lost from the

companion. Material spiraling in from the companion star along the black sequence of points in the right panel of Fig. 1 must therefore jump to one of the two blue sequences before proceeding inwards to the BH³.

The lower blue sequence represents a solution in which the disc angular momentum is anti-aligned with the BH spin at small radii ($\phi = \phi_\bullet - \pi$) and anti-aligned with the orbital angular momentum of the companion at large radii. This is equivalent to a solution in which the obliquity is 120° and the disc angular momentum is aligned with the BH spin at small radii and the companion's orbital angular momentum at large radii. Thus a smooth surface similar to the classical Laplace surface seen in the left panel of Fig. 1 exists around a spinning BH if and only if the obliquity exceeds 90° .

These conclusions raise two obvious questions: how is this unusual behavior related to the standard Bardeen–Petterson analysis of a warped accretion disc orbiting a spinning BH? And how do warped accretion discs actually behave in real astrophysical systems?

1.3 An approximate analysis of viscous warped discs

To show the relation between the findings of the preceding subsection and the Bardeen–Petterson treatment of viscous warped discs, we examine the approximate strength of the torques from various sources.

Suppose that the disc is strongly warped near some radius r . The torque per unit mass due to a companion is (eq. 4)

$$T_\star \simeq \frac{GM_\star r^2}{r_\star^3}, \quad (11)$$

where we have neglected all factors of order unity. Similarly, the torque from the quadrupole moment of the central body is (eq. 2)

$$T_p \simeq \frac{GMJ_2 R_p^2}{r^3}, \quad (12)$$

and the Lense–Thirring torque is (eq. 3)

$$T_{\text{LT}} \simeq \frac{R_g^{5/2} c^2 a_\bullet}{r^{5/2}}. \quad (13)$$

The torque per unit mass due to viscous stress is $T_v \simeq \eta\Omega/\rho$ where η is the viscosity and ρ is the density in the disc. In the Shakura–Sunyaev α -model of viscosity (eq. 26) $\eta = \alpha\rho c_s^2$ where c_s is the sound speed, and α is a constant, typically assumed to be ~ 0.1 . However, the Shakura–Sunyaev model was developed to model viscous forces in the disc arising from Keplerian shear, whereas the warp shape is determined by viscous forces due to much smaller shears normal to the disc plane. To represent the second kind of force we use an α -model with a different parameter α_\perp (for small-amplitude warps $\alpha_\perp = \frac{1}{2}\alpha^{-1}$; see eq. 33). Thus

$$T_v \simeq \alpha_\perp c_s^2. \quad (14)$$

For simplicity we shall usually assume that the disc is isothermal, in which case the viscous torque is independent of radius. Finally, the torque per unit mass due to the self-gravity of the disc is roughly

$$T_{sg} \simeq \pi G \Sigma r. \quad (15)$$

where Σ is the surface density near radius r .

Viscous quadrupole discs with a companion The quadrupole torque T_p decreases with radius, while the torque from the companion T_\star increases with radius. The two are equal at

$$r_w \simeq \left(J_2 \frac{M}{M_\star} R_p^2 r_\star^3 \right)^{1/5}. \quad (16)$$

which agrees with the precise definition of the warp radius in equation (6) to within a factor of order unity. Since the viscous torque T_v is independent of radius in an isothermal disc, and one of T_\star , T_p is always larger than $T_\star(r_w)$, the viscous torque is always smaller than the torque due to the central body or the companion if $\beta\alpha_\perp < 1$, where

$$\beta \equiv \frac{T_v/\alpha_\perp}{T_\star(r_w)} = \frac{c_s^2 R_p}{GMJ_2^{2/5}} \left(\frac{r_\star}{R_p} \right)^{9/5} \left(\frac{M}{M_\star} \right)^{3/5}. \quad (17)$$

This agrees with the precise definition of β that we give later in the paper (eq. 30) to within 1 per cent. In the terminology introduced at the start of the paper, a disc with $\beta\alpha_\perp \lesssim 1$ is a ‘low-viscosity’ disc.

³ J. Touma (private communication) points out that the time evolution of the orbit normals in the Lense–Thirring disc is the same as that of Colombo’s top, which describes the behavior of the spin axis of the Moon due to the torque from the Earth on the lunar figure and precession of the lunar orbit due to the Sun (Colombo 1966; Henrard & Murigande 1987). The solutions shown in the right panel of Fig. 1 correspond to the Cassini states of the Moon, of which there are two or four depending on whether the lunar semimajor axis is less than or greater than 34 Earth radii (Ward 1975).

Viscous Lense–Thirring discs with a companion The Lense–Thirring torque T_{LT} and the companion torque T_* are equal at

$$r_w \simeq \left(a_\bullet \frac{M}{M_*} R_g^{3/2} r_*^3 \right)^{2/9}, \quad (18)$$

and the ratio of the viscous torque to the Lense–Thirring or companion torque at r_w is then β_{α_\perp} where

$$\beta \equiv \frac{T_v/\alpha_\perp}{T_*(r_w)} = \frac{c_s^2}{c^2 a_\bullet^{4/9}} \left(\frac{r_*}{R_g} \right)^{5/3} \left(\frac{M}{M_*} \right)^{5/9}, \quad (19)$$

consistent with the precise definition in equation (30) to within 15 per cent.

We expect that the shape of a low-viscosity disc ($\beta_{\alpha_\perp} \lesssim 1$) is determined by the competition between the torque from the central body (quadrupole or Lense–Thirring torque) and the torque from the companion, rather than by viscous torques. On the other hand the surface-density distribution in a warped disc is always determined by the viscous torque, no matter how small, since the other two torques both scale linearly with the surface density and hence do not establish the surface-density distribution.

The usual Bardeen–Petterson description implicitly assumes that $\beta_{\alpha_\perp} \gg 1$ and neglects the companion torque. In this case the warp will be strongest at a smaller radius r'_w given by

$$r'_w \simeq \begin{cases} r_w/(\alpha_\perp \beta)^{1/3} \simeq (J_2 R_p^2 GM/\alpha_\perp c_s^2)^{1/3}; & \text{quadrupole disc} \\ r_w/(\alpha_\perp \beta)^{2/5} \simeq (a_\bullet/\alpha_\perp)^{2/5} (c/c_s)^{4/5} R_g & \text{Lense–Thirring disc.} \end{cases} \quad (20)$$

Viscous Lense–Thirring discs with self-gravity In accretion discs surrounding supermassive BHs at the centres of galaxies, there is no companion body (except in the case of a binary BH; see §5.2.1). Thus the torque T_* can be neglected. However, the disc can be massive enough that its self-gravity plays a role in determining its shape. In plausible disc models the surface density falls off slowly enough that this torque increases outward (see §5.2), and equals the Lense–Thirring torque at

$$r_w \simeq \left[\frac{a_\bullet R_g^{5/2} c^2}{\pi G \Sigma(r_w)} \right]^{2/7}; \quad (21)$$

note that this is an implicit equation for the warp radius r_w since the surface density depends on radius. The ratio of the viscous torque, equation (14), to the Lense–Thirring and self-gravity torques at r_w is then γ_{α_\perp} , where

$$\gamma \equiv \frac{T_v/\alpha_\perp}{T_{sg}(r_w)} = \frac{c_s^2}{\pi G \Sigma r} \Big|_{r_w}. \quad (22)$$

Note that $\gamma \simeq Q(H/r)$ where Q is Toomre’s parameter (eq. 69) and $H = c_s/\Omega$ is the disc thickness. Thus the viscosity becomes low (in the sense that $\gamma \ll 1$) in thin discs ($H/r \ll 1$) long before they become gravitationally unstable ($Q < 1$).

2 EVOLUTION OF VISCOUS DISCS WITH COMPANIONS

2.1 Evolution equations

The equations that describe the evolution of a warped, thin accretion disc are derived by Pringle (1992), Ogilvie (1999), and Ogilvie & Latter (2013a). Our starting point is Ogilvie (1999)’s equations (121) and (122). The first of these is the equation of continuity

$$2\pi r \frac{\partial \Sigma}{\partial t} + \frac{\partial C_M}{\partial r} = 0, \quad C_M \equiv 2\pi r \Sigma v_r, \quad (23)$$

where $\Sigma(r, t)$ is the surface density, $v_r(r, t)$ is the radial drift velocity, and $C_M(r, t)$ is the mass current (rate of outward flow of disc mass through radius r). The second is an equation for angular momentum conservation,

$$2\pi r \frac{\partial \mathbf{L}}{\partial t} + \frac{\partial \mathbf{C}_L}{\partial r} = 2\pi r \Sigma \mathbf{T}, \quad (24)$$

where $\Omega(r) \equiv (GM/r^3)^{1/2}$ is the Keplerian angular speed, $\mathbf{L} = \Sigma r^2 \Omega \hat{\mathbf{n}}$ is the angular momentum per unit area, \mathbf{T} is the torque per unit mass from sources external to the disc, and \mathbf{C}_L is the angular-momentum current, given by the sum of advective and viscous currents,

$$\mathbf{C}_L \equiv \mathbf{C}_{\text{adv}} + \mathbf{C}_{\text{visc}},$$

$$\begin{aligned} \mathbf{C}_{\text{adv}}(r, t) &= 2\pi r^3 \Omega \Sigma v_r \hat{\mathbf{n}} = r^2 \Omega \hat{\mathbf{n}} C_M, \\ \mathbf{C}_{\text{visc}}(r, t) &= -2\pi r^2 \Sigma c_s^2 \left(Q_1 \hat{\mathbf{n}} + Q_2 r \frac{\partial \hat{\mathbf{n}}}{\partial r} + Q_3 r \hat{\mathbf{n}} \times \frac{\partial \hat{\mathbf{n}}}{\partial r} \right). \end{aligned} \quad (25)$$

Here c_s is the sound speed, which is constant in an isothermal disc (as we shall assume from now on), and as usual $\hat{\mathbf{n}}(r, t)$ is the unit vector normal to the disc at radius r . The dimensionless coefficients Q_1, Q_2, Q_3 depend on the equation of state, the viscosity, and the warp $\psi \equiv r|\partial\hat{\mathbf{n}}/\partial r|$. For a flat Keplerian disc, Q_1 is related to the kinematic viscosity by $\nu = -\frac{2}{3}Q_1c_s^2/\Omega$ and the mean-square height of the disc above the midplane is $H^2 = c_s^2/\Omega^2$.

These equations are based on the assumptions (Ogilvie 1999) that (i) the disc is thin, $H/r \ll 1$; (ii) the fluid obeys the compressible Navier–Stokes equation; (iii) the fluid equation of state is barotropic, i.e., the viscosity is dynamically important but not thermodynamically important; (iv) the disc is non-resonant in the sense of equation (1). In the calculations below we shall also assume that (v) the viscosity is described by the Shakura–Sunyaev α -model, that is, the shear and bulk viscosities η and ζ are related to the pressure p by

$$\eta = \alpha p/\Omega, \quad \zeta = \alpha_b p/\Omega, \quad (26)$$

where α and α_b are constants. For a flat, isothermal disc the kinematic viscosity is $\nu = \eta/\rho = \alpha c_s^2/\Omega$, so $\alpha = -\frac{2}{3}Q_1$.

Now take the scalar product of (24) with $\hat{\mathbf{n}}$. Since $\hat{\mathbf{n}} \cdot \hat{\mathbf{n}} = 1$, $\hat{\mathbf{n}} \cdot \partial\hat{\mathbf{n}}/\partial t = \hat{\mathbf{n}} \cdot \partial\hat{\mathbf{n}}/\partial r = 0$. Moreover $\hat{\mathbf{n}} \cdot \mathbf{T} = 0$ for the Lense–Thirring torque and for any torque arising from a gravitational potential, so we shall assume that this condition holds in general. We also use equation (23) to eliminate $\partial\Sigma/\partial t$. The result is an expression for the mass current,

$$C_M = 2\pi r \Sigma v_r = -\frac{2}{r\Omega} \hat{\mathbf{n}} \cdot \frac{\partial \mathbf{C}_{\text{visc}}}{\partial r} = \frac{4\pi c_s^2}{r\Omega} \frac{\partial}{\partial r} (\Sigma r^2 Q_1) - \frac{4\pi \Sigma c_s^2 r^2}{\Omega} Q_2 \left| \frac{\partial \hat{\mathbf{n}}}{\partial r} \right|^2. \quad (27)$$

We now introduce several new variables: the dimensionless radius $x \equiv r/r_w$ with the warp radius r_w given by (6) or (9); the dimensionless time $\tau \equiv t c_s^2/(GM r_w)^{1/2}$ (roughly, for a Shakura–Sunyaev disc with $\alpha \sim 1$ this is time measured in units of the viscous diffusion time at the warp radius); and $y(r, t) \equiv \Sigma(r, t)(GM r_w)^{1/2}$ (with dimensions of angular momentum per unit area). Equation (24) becomes

$$\frac{\partial \mathbf{L}}{\partial \tau} + \frac{1}{x} \frac{\partial}{\partial x} (\mathbf{c}_{\text{visc}} + x^{1/2} c_M \hat{\mathbf{n}}) = \frac{y}{\beta} \begin{cases} x^2 (\hat{\mathbf{n}} \cdot \hat{\mathbf{n}}_*) \hat{\mathbf{n}} \times \hat{\mathbf{n}}_* + x^{-3} (\hat{\mathbf{n}} \cdot \hat{\mathbf{n}}_p) \hat{\mathbf{n}} \times \hat{\mathbf{n}}_p & \text{quadrupole} \\ x^2 (\hat{\mathbf{n}} \cdot \hat{\mathbf{n}}_*) \hat{\mathbf{n}} \times \hat{\mathbf{n}}_* - x^{-5/2} \hat{\mathbf{n}} \times \hat{\mathbf{n}}_* & \text{Lense–Thirring} \end{cases} \quad (28)$$

where $\hat{\mathbf{n}} = \mathbf{L}/|\mathbf{L}| = \mathbf{L}/(\Sigma r^2 \Omega) = \mathbf{L}/(y x^{1/2})$, $y = |\mathbf{L}|/x^{1/2}$,

$$\mathbf{c}_{\text{visc}} \equiv \frac{1}{2\pi c_s^2} \left(\frac{GM}{r_w^3} \right)^{1/2} \mathbf{C}_{\text{visc}} = -y x^2 \left(Q_1 \hat{\mathbf{n}} + Q_2 x \frac{\partial \hat{\mathbf{n}}}{\partial x} + Q_3 x \hat{\mathbf{n}} \times \frac{\partial \hat{\mathbf{n}}}{\partial x} \right),$$

$$c_M \equiv \frac{GM}{2\pi r_w c_s^2} C_M = -2x^{1/2} \hat{\mathbf{n}} \cdot \frac{\partial \mathbf{c}_{\text{visc}}}{\partial x} = 2x^{1/2} \left[\frac{\partial}{\partial x} (y x^2 Q_1) - y x^3 Q_2 \left| \frac{\partial \hat{\mathbf{n}}}{\partial x} \right|^2 \right]. \quad (29)$$

The dimensionless parameter β is given by

$$\beta \equiv \frac{4M}{3M_*} \frac{c_s^2 r_w}{GM} \left(\frac{r_*}{r_w} \right)^3 = \begin{cases} \frac{2^{8/5} c_s^2 R_p}{3J_2^{2/5} GM} \left(\frac{r_*}{R_p} \right)^{9/5} \left(\frac{M}{M_*} \right)^{3/5} & \text{quadrupole} \\ \frac{2^{2/3}}{3^{5/9} a_*^{4/9}} \frac{c_s^2}{c^2} \left(\frac{r_*}{R_g} \right)^{5/3} \left(\frac{M}{M_*} \right)^{5/9} & \text{Lense–Thirring} \end{cases} \quad (30)$$

and represents the ratio of the strength of the viscous torque to the external torque at the characteristic warp radius r_w (cf. eqs. 17 and 19).

Equation (28) is a parabolic partial differential equation for the three components of \mathbf{L} . The dimensionless viscosity coefficients Q_i are functions of the equation of state and of the warp $\psi \equiv x|\partial\hat{\mathbf{n}}/\partial x|$ (Ogilvie 1999). Ogilvie shows that for an isothermal α -disc and small warps ($\psi \ll 1$),

$$Q_1 = -\frac{3\alpha}{2} + \mathcal{O}(\psi^2), \quad Q_2 = \frac{1+7\alpha^2}{\alpha(4+\alpha^2)} + \mathcal{O}(\psi^2) = \frac{1}{4\alpha} + \mathcal{O}(\alpha, \psi^2). \quad (31)$$

We shall also examine a simplified set of equations that appear to contain most of the important physics of equations (28)–(30). In these equations (i) we examine only the steady-state disc, that is, we set $\partial\mathbf{L}/\partial t = 0$ in equation (28); (ii) we set $Q_3 = 0$, since it appears to play no important role in the dynamics; and (iii) we neglect the dependence of Q_1 and Q_2 on the warp ψ , that is, we treat them as constants. The steady-state assumption implies that the mass current c_M is a constant of the problem, independent of radius. We have

$$\frac{dy}{dx} + y \left(\frac{2}{x} - \frac{Q_2 x}{Q_1} \left| \frac{d\hat{\mathbf{n}}}{dx} \right|^2 \right) = \frac{c_M}{2Q_1 x^{5/2}},$$

$$\begin{aligned} \frac{d^2 \hat{\mathbf{n}}}{dx^2} + \frac{d\hat{\mathbf{n}}}{dx} \left[\frac{Q_1/Q_2 + 3}{x} - \frac{c_M}{Q_2 x^{5/2} y} + \frac{d \log y}{dx} \right] + \left| \frac{d\hat{\mathbf{n}}}{dx} \right|^2 \hat{\mathbf{n}} \\ = -\frac{1}{\beta Q_2} \begin{cases} (\hat{\mathbf{n}} \cdot \hat{\mathbf{n}}_*) \hat{\mathbf{n}} \times \hat{\mathbf{n}}_* + x^{-5} (\hat{\mathbf{n}} \cdot \hat{\mathbf{n}}_p) \hat{\mathbf{n}} \times \hat{\mathbf{n}}_p & \text{quadrupole} \\ (\hat{\mathbf{n}} \cdot \hat{\mathbf{n}}_*) \hat{\mathbf{n}} \times \hat{\mathbf{n}}_* - x^{-9/2} \hat{\mathbf{n}} \times \hat{\mathbf{n}}_* & \text{Lense–Thirring} \end{cases} \end{aligned} \quad (32)$$

The three components of the unit vector $\hat{\mathbf{n}}$ are related by the constraint $|\hat{\mathbf{n}}| = 1$.

This simplified model is similar to Pringle’s (1992) equations of motion, in which there are two viscosities η and η_\perp (in Pringle’s notation, these are $\rho\nu_1$ and $\rho\nu_2$), the first of which is associated with the Keplerian shear and the second with shear perpendicular to the disc caused by a warp. In an α -disc model $\eta = \alpha\rho c_s^2$ and $\eta_\perp = \alpha_\perp\rho c_s^2$ and the two models are equivalent if

$$Q_1 = -\frac{3\alpha}{2}, \quad Q_2 = \frac{\alpha_\perp}{2}. \quad (33)$$

If $\alpha \ll 1$ and the warp is small, equation (31) implies that $\alpha_\perp = \frac{1}{2}\alpha^{-1}$ (Papaloizou & Pringle 1983; Ogilvie 1999).

Although we adopt this formalism, one should keep in mind that angular-momentum transport in real accretion discs is thought to be driven by MHD turbulence, which may not be well approximated by an isotropic viscosity – or if it is, the viscosity may not be well approximated by the Shakura–Sunyaev α -model. Some support for this formalism is provided by local, non-relativistic MHD simulations that examine the decay of an imposed epicyclic oscillation (Torkelsson et al. 2000). Global, general-relativistic MHD simulations have tended to show solid-body precession rather than Bardeen–Petterson alignment, although most of these correspond to the resonant regime $\alpha < H/r$ (cf. eq. 1), which we exclude (e.g. Fragile et al. 2007). More recently, global but non-relativistic MHD calculations with an approximate treatment of Lense–Thirring precession have been performed by Sorathia et al. (submitted to ApJ; see also Sorathia et al. 2013). They find that diffusive damping of vertical shear is much less important than the derivation of the Pringle–Ogilvie equations implies. This in turn implies that the Pringle–Ogilvie + Shakura–Sunyaev formalism overestimates the strength of viscous torques when $\alpha \ll 1$ and so the importance of tidal torques and self-gravity in accretion discs is even greater than we find below.

2.2 Numerical methods

Steady-state discs We have solved the simplified ordinary differential equations (32) for steady-state discs with constant viscosity coefficients and $Q_3 = 0$. We find the numerical solution over a range of dimensionless radii $[x_a, x_b]$; typically we choose $x_b = 1/x_a = 30$, although in some cases where the viscosity is large we cover a larger range to ensure that the disc is not still warped at either end of the integration range. The viscosity coefficients Q_1 and Q_2 are usually fixed at their values for an unwarped disc with $\alpha = 0.2$, $\alpha_b = 0$, in which case $Q_1 = -0.3$, $Q_2 = 1.58416$. The equations are unchanged under the rescaling $y(x) \rightarrow \lambda y(x)$, $c_M \rightarrow \lambda c_M$, so the normalization of the mass current c_M can be chosen arbitrarily apart from the sign. We are interested in the case in which mass flows into the BH, so we set $c_M = -1$.

Seven boundary conditions are required for the one first-order and three second-order equations. In the region $x \ll 1$ where external torques are negligible, the disc is assumed to be flat, $d\hat{\mathbf{n}}/dx = 0$. Then the first of equations (32) has the solution

$$y(x) = \frac{c_M}{Q_1 x^{3/2}} + \frac{k}{x^2}, \quad (34)$$

where k is an integration constant. We assume a no-torque boundary condition at the radius x_{ISCO} of the innermost stable circular orbit, which is close to the BH; this requires that the viscous angular-momentum current $\mathbf{c}_{\text{visc}} = 0$ at x_{ISCO} and from the first of equations (29) this in turn requires $y = 0$ at x_{ISCO} . Thus

$$y(x) = \frac{c_M}{Q_1 x^2} (x^{1/2} - x_{\text{ISCO}}^{1/2}). \quad (35)$$

We assume that the inner boundary of our integration region x_a is much larger than x_{ISCO} so in the region of interest

$$y(x) = \frac{c_M}{Q_1 x^{3/2}}, \quad (36)$$

which provides one boundary condition at $x = x_a$.

At the outer radius x_b the disc should lie in the plane of the companion-star orbit, as we would expect if the disc is fed by mass loss from the companion. Thus $\hat{\mathbf{n}} = \hat{\mathbf{n}}_*$ at $x = x_b$, which provides three additional boundary conditions. Moreover since $|\hat{\mathbf{n}}| = 1$ at all radii, we must have $\hat{\mathbf{n}} \cdot \partial\hat{\mathbf{n}}/\partial x = 0$ at $x = x_b$, which provides another boundary condition (it is straightforward to show from the second of eqs. 32 that these conditions are sufficient to ensure that $|\hat{\mathbf{n}}| = 1$ at all radii). Note that we do not require that the disc lies in the equator of the central body for $x \ll 1$, although it turns out to do so in all of our numerical solutions.

Let us assume for simplicity that (i) inside the inner integration boundary x_a the external torques on the right side of the second of equations (32) vanish; (ii) the disc normal $\hat{\mathbf{n}}$ is nearly constant, $\hat{\mathbf{n}}(x) = \hat{\mathbf{n}}_0 + \epsilon\hat{\mathbf{n}}_1(x)$ where $\epsilon \ll 1$. Then to first order in ϵ the first of equations (32) is the same as for a flat disc, yielding the solution (36). Substituting this result into the second of equations (32) and working to first order in ϵ we find

$$\frac{d^2\hat{\mathbf{n}}_1}{dx^2} + \frac{3}{2x} \frac{d\hat{\mathbf{n}}_1}{dx} = 0 \quad \text{with solution} \quad \hat{\mathbf{n}}_1 = \mathbf{a} + \mathbf{b}x^{-1/2} \quad (37)$$

where \mathbf{a} and \mathbf{b} are constants. To avoid an unphysical solution that grows as $x \rightarrow 0$ we must have $\mathbf{b} = 0$. The component of \mathbf{b} along $\hat{\mathbf{n}}$ is already guaranteed to be zero because our earlier boundary conditions ensure that $\hat{\mathbf{n}} \cdot d\hat{\mathbf{n}}/dx = 0$. Thus the

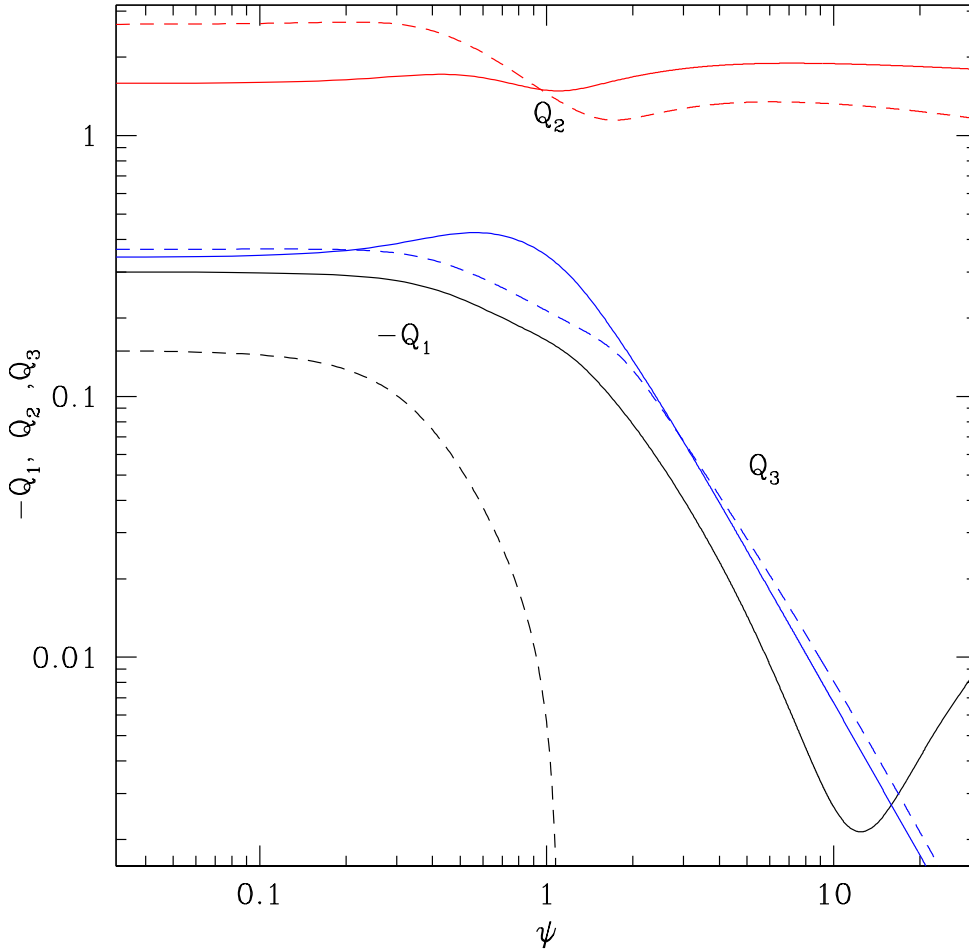


Figure 2. The viscosity coefficients $-Q_1$, Q_2 , Q_3 for an isothermal disc with viscosity described by a Shakura–Sunyaev α -model (eq. 26) having $\alpha = 0.2$, $\alpha_b = 0$ (solid lines) or $\alpha = 0.1$, $\alpha_b = 0.1$ (dashed lines). The horizontal coordinate is the dimensionless warp $\psi \equiv r|d\hat{\mathbf{n}}/dr|$. We plot $-Q_1$ because Q_1 is normally negative for small warps; for $\alpha = 0.2$, $\alpha_b = 0$ Q_1 is negative for all ψ while for $\alpha = 0.1$, $\alpha_b = 0.1$ Q_1 is positive for $\psi > 1.106$. The calculations follow the precepts of Ogilvie (1999) and employ a code provided by G. Ogilvie.

two components of $d\hat{\mathbf{n}}/dx$ perpendicular to $\hat{\mathbf{n}}$ must vanish at the inner boundary x_a , which provides the final two boundary conditions. Note that there is no similar requirement at the outer boundary, since the parasitic solution $\mathbf{b}x^{-1/2}$ decays as $x \rightarrow \infty$.

The resulting boundary-value problem is solved using a collocation method with an adaptive mesh (routine D02TVF from Numerical Algorithms Group). To improve convergence we start with zero obliquity and increase the obliquity in steps of 1° , using the converged solution from each value of the obliquity as the initial guess for the solution for the next.

Time-dependent discs We have solved the partial differential equations (28), typically over the interval $[x_a, x_b]$ with $x_b = 1/x_a = 30$. Usually the viscosity coefficients Q_i are chosen to be appropriate for a disc with $\alpha = 0.2$, $\alpha_b = 0$. The coefficients are determined as functions of the warp $\psi \equiv x|\partial\hat{\mathbf{n}}/\partial x|$ using a code generously provided by G. Ogilvie (see Fig. 2); the coefficients are tabulated on a grid $0 \leq \psi \leq 10$ and interpolated using cubic splines. Mass, and the corresponding angular momentum for circular orbits, are added at a constant rate with a Gaussian distribution in radius centred at $x = 10$ (i.e., well outside the warp) and the disc is followed until it reaches a steady state. The integration is carried out using the routine D03PCF from Numerical Algorithms Group. A complication is that the dependence of the coefficient Q_1 on ψ means that equation (28) is third-order in the spatial derivative; to reduce this to a second-order equation we treat the mass current c_M as a fourth dependent variable in addition to the three components of the angular momentum \mathbf{L} and integrate the second of equations (29) along with equations (28).

As in the steady-state case we assume that the disc is aligned with the companion-star orbit at large radii, so $\hat{\mathbf{n}} = \hat{\mathbf{n}}_*$ at the outer boundary $x = x_b$. We also assume that the steady-state relation (36) between the surface density and the mass current in a flat disc applies at the inner boundary x_a ; this is plausible since we expect the disc to achieve an approximate

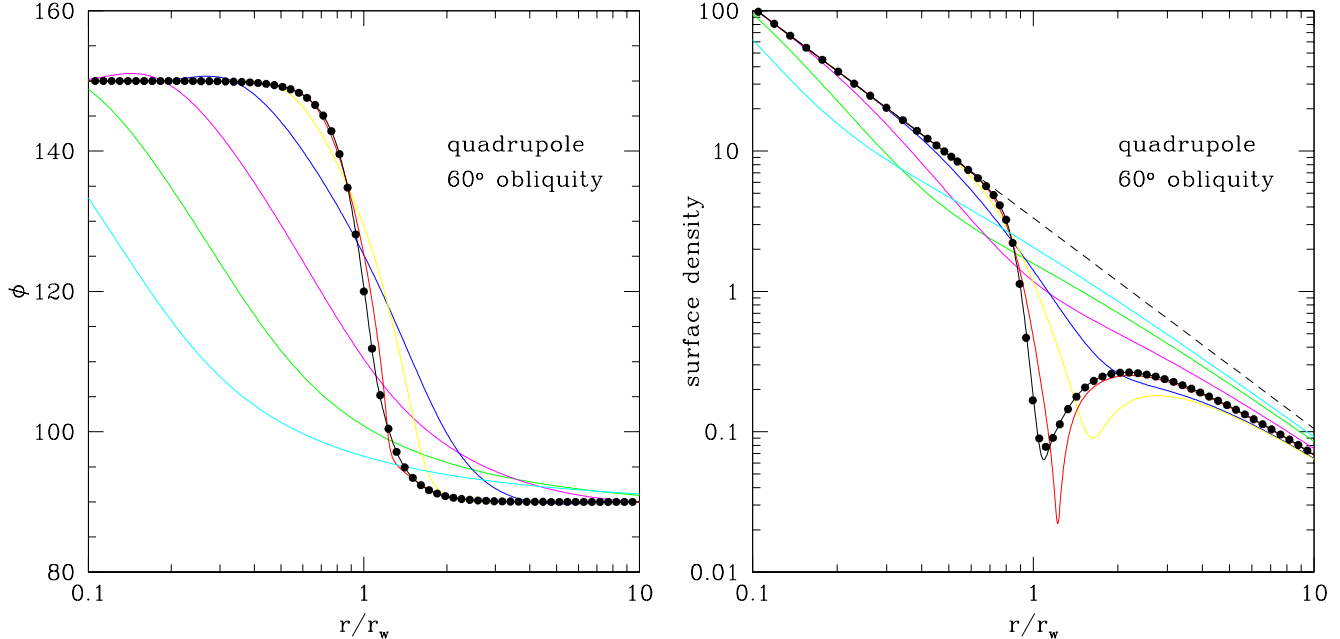


Figure 3. (left) The orientation of a stationary disc orbiting a planet that has an obliquity of 60° (from eqs. 32). The viscosity coefficients are $Q_1 = -0.3$, $Q_2 = 1.58416$, appropriate for a flat disc with $\alpha = 0.2$, $\alpha_b = 0$, and the mass current is $c_M = -1$. The solutions shown have the parameter β (eq. 30) representing the ratio of viscous torques to external torques equal to 1000 (cyan), 100 (green), 10 (magenta), 1 (blue), 0.1 (yellow), 0.01 (red), 0.001 (black). The solid black circles represent the inviscid solution (the Laplace surface), given by equation (6) and shown in the left panel of Fig. 1. (right) The surface density $y(x)$ for the discs shown in the left panel. The solid circles show the solution given by the first of equations (32) and the orientation $\hat{\mathbf{n}}(x)$ of the inviscid disc. The dashed line shows the surface density for a flat disc (eq. 36).

steady-state most rapidly at small radii. We assume that there is an outer disc boundary $x_o \gg x_b$ at which a no-torque boundary condition applies. In the steady-state disc, arguments analogous to those leading to equations (34)–(36) imply

$$y(x) = -\frac{c_M}{Q_1 x^2} (x_o^{1/2} - x^{1/2}). \quad (38)$$

This implies in turn that at the outer boundary

$$y(x_b) = -\frac{c_M}{Q_1 x_b^2} (x_o^{1/2} - x_b^{1/2}) \quad \text{and} \quad \mathbf{c}_L = c_M x_o^{1/2} \hat{\mathbf{n}}_*. \quad (39)$$

Typically we use $x_o = 10x_b$. Finally, the angular-momentum current at x_{ISCO} is $\mathbf{c}_L = x_{\text{ISCO}}^{1/2} c_M \hat{\mathbf{n}}$ which can be taken to be zero since x_{ISCO} is very small. Since the disc is flat inside the warp radius and the inner integration boundary x_a is much less than the warp radius, we may assume that \mathbf{c}_L is constant between x_{ISCO} and x_a so we set $\mathbf{c}_L(x_a) = 0$.

We usually start with a low-density disc and zero obliquity, and add mass and angular momentum outside the warp radius at a constant rate until the disc reaches a steady state; then we slowly increase the obliquity to the desired value.

2.3 Results

Quadrupole discs The left panel of Fig. 3 shows the solutions of equation (32) for a planet obliquity of 60° and a range of viscosity parameters β from 1000 to 0.001. As one might expect, very viscous discs ($\beta \gg 1$) exhibit a smooth, gradual warp while low-viscosity discs ($\beta \ll 1$) are close to the inviscid disc (eq. 6), shown as the solid circles.

The right panel shows the surface density $y(x)$. Here the behavior is more interesting. While the surface density in very viscous discs is close to that of a flat disc (dashed line, from eq. 36), as the viscosity is lowered the disc develops a sharp valley – almost two orders of magnitude – in the surface density near the warp radius r_w . The valley presumably occurs because the viscous stresses are larger when the warp $\psi = x|d\hat{\mathbf{n}}/dx|$ is large, so the mass and angular-momentum current can be carried by a smaller surface density. The asymptotic behavior of the surface density as the viscosity becomes small is obtained from the first of equations (32) by substituting for $|d\hat{\mathbf{n}}/dx|$ the value from the inviscid solution (6); this is shown as the solid circles in the right panel of Fig. 3.

The nature of the surface-density valley associated with the warp is illustrated further in Fig. 4, which shows the surface-density profile for low-viscosity discs ($\beta \rightarrow 0$) for obliquities $10^\circ, 20^\circ, \dots, 80^\circ$. As the obliquity grows the valley becomes

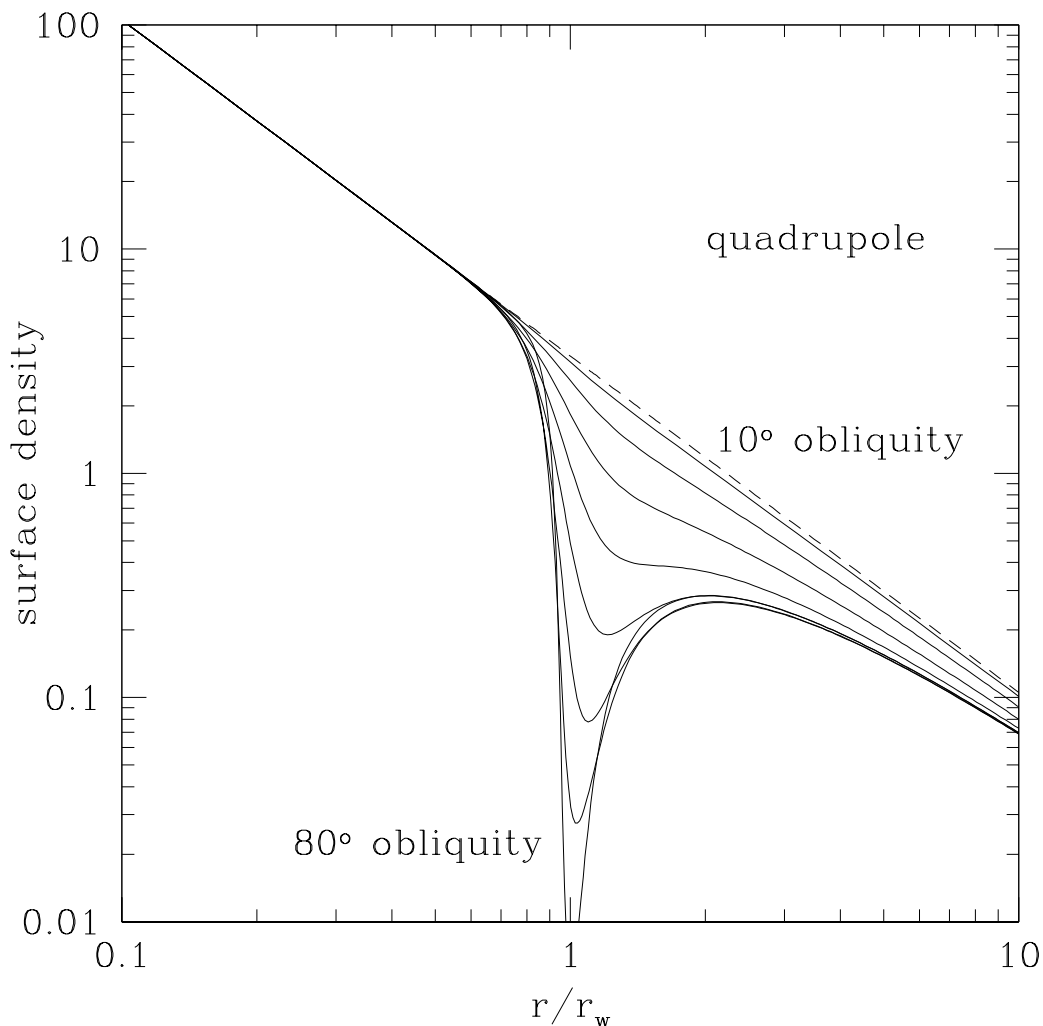


Figure 4. The surface density $y(x)$ for quadrupole discs with negligible viscosity ($\beta \rightarrow 0$) and obliquity $10^\circ, 20^\circ, \dots, 80^\circ$. The other parameters of the discs are the same as in Fig. 3. The dashed line shows the surface density for a flat disc (eq. 36).

deeper: at an obliquity of 80° the surface density is only 0.2 per cent of the surface density in an unwarped disc at the bottom of the valley, near radius $1.00r_w$.

The steady-state warped discs also exhibit some spirality or twisting; this is shown in Fig. 5 by plotting the horizontal components (n_x, n_y) of the unit vector normal to the disc.

Lense–Thirring discs Fig. 6 is analogous to Fig. 3: it shows the solutions of equation (32) for a Lense–Thirring disc when the BH obliquity is 60° . The viscosity parameter β ranges from 1000 to 0.333; for $\beta < 0.333$ no steady-state solution exists. Similarly, the right panel of Fig. 6 shows the horizontal components of the unit normal in Lense–Thirring discs with 60° , to be compared with the left panel of the same figure for quadrupole discs.

The absence of steady-state solutions for Lense–Thirring discs for viscosity less than some critical value at fixed obliquity – or obliquity larger than a critical value at fixed viscosity – is a novel feature not seen in the quadrupole discs, and presumably related to the jump seen in the orientation of inviscid Lense–Thirring discs (§1.2).

Fig. 7 illustrates how the critical obliquity and viscosity parameter are related. The black curve shows the critical values for the simplified steady-state equations (32), with $Q_1 = -0.3$, $Q_2 = 1.58416$, $Q_3 = 0$. The critical values are defined here by the point where the maximum warp $\psi = 10$; this is generally close to the curve with $\psi \rightarrow \infty$ and for $\psi \gtrsim 10$ it is unlikely that our model is accurate in any case.

The red curve in Fig. 7 shows the critical values obtained by solving the time-dependent equations (28) for the same constant values of Q_i ; in this case the critical values are defined by the obliquity at which the maximum warp of the time-dependent solution exceeds $\psi = 10$. The agreement of the red and black curves is partly a successful check of our steady-state and time-dependent numerical codes, but more importantly it implies that time-dependent discs with obliquity above the

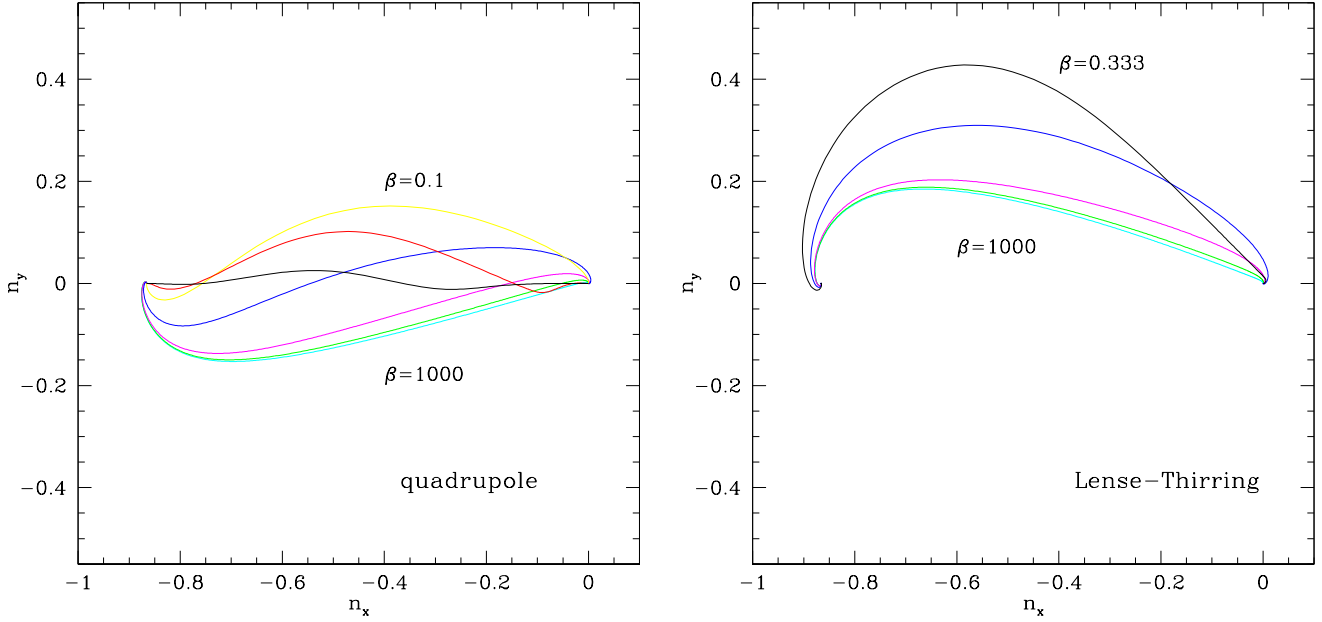


Figure 5. The horizontal components (n_x, n_y) of the unit normal vector for quadrupole discs (left panel) and Lense-Thirring discs (right panel). The obliquity is 60° and the other parameters are as described in Fig. 3 (left panel) or 6 (right panel). In both panels the parameter β (eq. 30), representing the ratio of viscous torques to external torques, is equal to 1000 (cyan), 100 (green), 10 (magenta), 1 (blue); in the left panel there are additional curves for $\beta = 0.1$ (yellow), 0.01 (red), 0.001 (black) and in the right panel there is an additional curve for the critical value $\beta = 0.333$ (black).

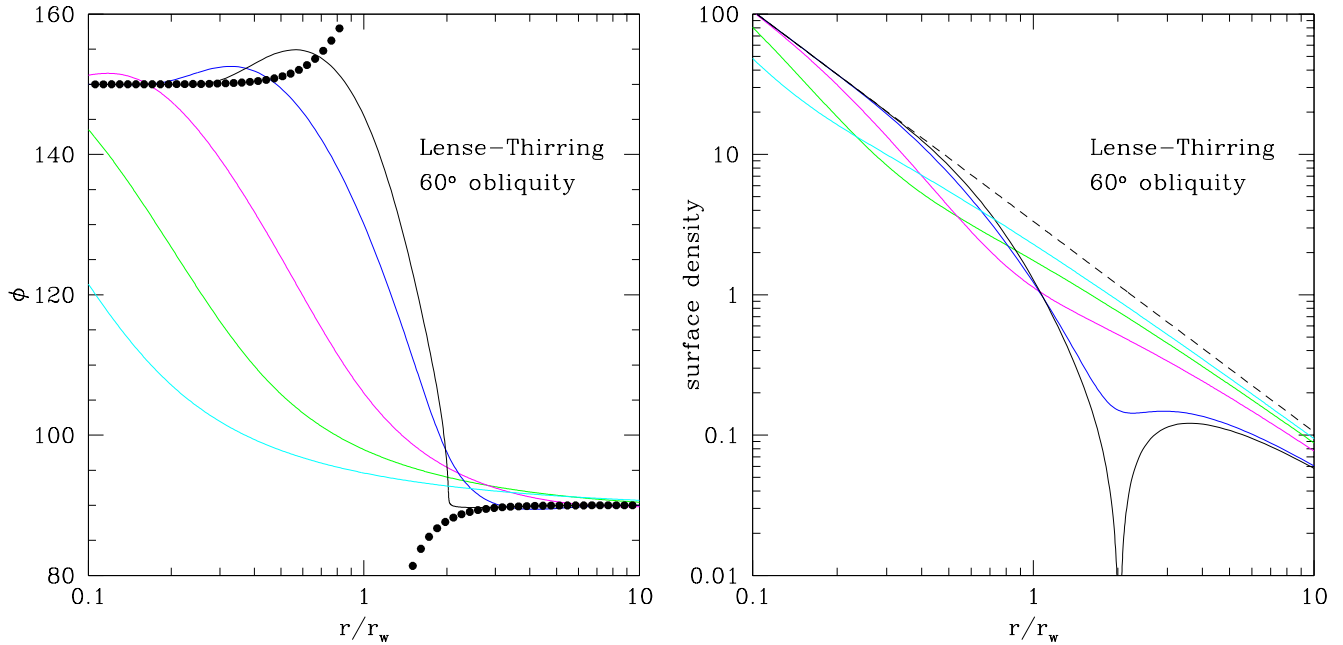


Figure 6. (left) The orientation of a stationary disc orbiting a BH that has an obliquity of 60° (from eqs. 32). The parameters are the same as in Fig. 3, except that the parameter β (eq. 30) representing the ratio of viscous torques to external torques equals 1000 (cyan), 100 (green), 10 (magenta), 1 (blue), and 0.333 (black). For $\beta < 0.333$ no solution exists. The solid black circles represent the inviscid solution, given by equation (9) and shown in the right panel of Fig. 1. (right) The surface density $y(x)$ for the discs shown in the left panel. The dashed line shows the surface density for a flat disc (eq. 36).

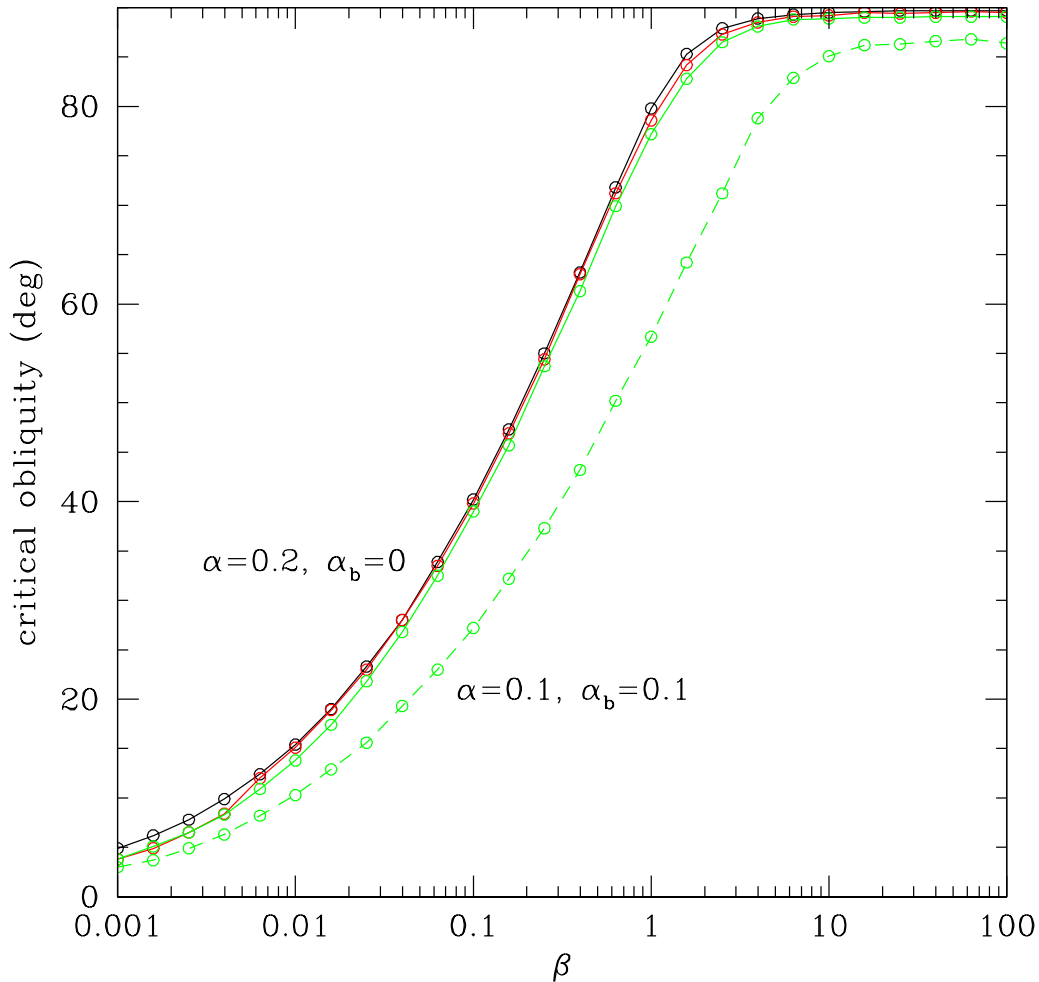


Figure 7. Above the critical obliquity shown here, steady-state Lense–Thirring disc solutions do not exist. The parameter β measures the strength of the viscous forces (eq. 30). The solid lines are for Shakura–Sunyaev discs with $\alpha = 0.2$, $\alpha_b = 0$ and the dashed line is for $\alpha = \alpha_b = 0.1$. The black and red curves are derived from steady-state and time-dependent disc models (eqs. 28 and 32) with the viscosity parameters Q_1 and Q_2 set to their unwarped values and $Q_3 = 0$. The green curves are for Q_i depending on the local warp, as in Fig. 2.

critical value will develop singular warps – that is, for example, there is no oscillating solution of the time-dependent Pringle–Ogilvie equations that remains non-singular.

The green curve shows the critical values obtained from equations (28) with viscosity parameters Q_i that depend on the warp as shown in Fig. 2. This exhibits the same qualitative behavior as the black and red curves, demonstrating that the critical values are not strongly dependent on the variation of viscosity parameters with the strength of the warp.

Finally, the green dashed curve is the same as the green solid curve, but for parameters Q_i appropriate for Shakura–Sunyaev parameters $\alpha = 0.1$, $\alpha_b = 0.1$.

What happens to a Lense–Thirring accretion disc when the obliquity exceeds the critical value is not understood. Finite-time singularities (‘blow-up’) are a common feature of non-linear parabolic partial differential equations such as the Pringle–Ogilvie equations and it is likely that the absence of a solution reflects the approximation of the correct, hyperbolic, fluid equations with diffusion equations. The limitations of the diffusion approximation in warped discs are well-known: Papaloizou & Pringle (1983) argue that a transition from diffusive to wavelike behavior occurs when α decreased below H/r (see also Papaloizou & Lin 1995 and Ogilvie 2006). In this regime, bending waves governed by the pressure in the disk could transport angular momentum to connect smoothly the inner and outer disks. The behavior of such waves in Lense–Thirring discs is described by Lubow et al. (2002) but only to linear order in the warp amplitude, where the singular behavior is not present. For finite-amplitude warps, it is far from clear how to incorporate the required extra physics into the Pringle–Ogilvie equations or what behavior we might expect.

The sharp changes in disc orientation seen in Fig. 6 are reminiscent of the phenomenon of ‘breaking’ in which the

orientation of the accretion disc changes almost discontinuously (Nixon & King 2012; Nixon et al. 2012), although there are substantial differences in the phenomenology and interpretation (see §4 for further discussion).

2.4 The behavior of the disc at the critical obliquity

At the critical obliquity or viscosity there is a radius (the ‘critical radius’) at which the surface density approaches zero and the disc warp $\psi = r|d\psi/dr|$ changes from near zero to a very large value (black curves in Fig. 6). We can offer some analytic insight into this behavior.

Since the behavior of the disc changes sharply in a small radial distance, this change is unlikely to be due to the external torques, which vary smoothly with radius. Thus we examine the governing differential equations (28) with the right-hand side and $\partial/\partial\tau$ set to zero. Then this equation states that the total angular-momentum current $\mathbf{c}_{\text{visc}} + x^{1/2}c_M\hat{\mathbf{n}}$ must be independent of radius x . We erect a coordinate system specified by the triple of unit vectors $\hat{\mathbf{e}}_1, \hat{\mathbf{e}}_2, \hat{\mathbf{e}}_3$ with $\hat{\mathbf{e}}_3$ parallel to the angular-momentum current, so $\mathbf{c}_{\text{visc}} + x^{1/2}c_M\hat{\mathbf{n}} = c_L\hat{\mathbf{e}}_3$ with the mass and angular-momentum currents c_M and c_L constants. For simplicity we assume that the viscosity coefficients Q_1, Q_2 are constants, and $Q_3 = 0$. Then

$$x^{1/2}c_M\hat{\mathbf{n}} - Q_1x^2y(x)\hat{\mathbf{n}} - Q_2x^3y(x)\frac{d\hat{\mathbf{n}}}{dx} = c_L\hat{\mathbf{e}}_3. \quad (40)$$

Since $\hat{\mathbf{n}}$ is a unit vector, $\hat{\mathbf{n}} \cdot d\hat{\mathbf{n}}/dx = 0$, we may take the dot product with $\hat{\mathbf{n}}$ to obtain

$$x^{1/2}c_M - Q_1x^2y(x) = c_Lf(x) \quad \text{where} \quad f(x) \equiv \hat{\mathbf{n}} \cdot \hat{\mathbf{e}}_3 = n_3. \quad (41)$$

The components of (40) along $\hat{\mathbf{e}}_1$ and $\hat{\mathbf{e}}_2$ are

$$\left[x^{1/2}c_M - Q_1x^2y(x) \right] n_{1,2} - Q_2x^3y(x)\frac{dn_{1,2}}{dx} = 0. \quad (42)$$

Combining equations (41) and (42) with the conditions $\sum_{i=1}^3 n_i^2 = 1$, $\sum_{i=1}^3 n_i dn_i/dx = 0$, we find

$$\frac{df}{dx} = \frac{Q_1}{Q_2x} \frac{1 - f^2}{f - x^{1/2}c_M/c_L}. \quad (43)$$

The interesting behavior occurs if the mass and angular-momentum current have the same sign. In this case the non-linear differential equation (43) has a critical point at $f = 1$, $x = (c_L/c_M)^2 \equiv x_c$. If we restrict ourselves to the usual case in which $Q_1 < 0$, $Q_2 > 0$, then near the critical point solutions must take one of the following two forms:

(i) $f = 1$; this implies an unwarped disc with normal parallel to the angular-momentum current. The surface density is given by equation (41) as

$$y(x) = \frac{c_M}{2Q_1x_c^{5/2}}(x - x_c) + O(x - x_c)^2. \quad (44)$$

In the usual case where the mass current $c_M < 0$ this solution is physical (positive surface density) for $x > x_c$, i.e., outside the critical point.

(ii) In this case

$$f(x) = 1 + \frac{Q_2 - 4Q_1}{2Q_2x_c}(x - x_c) + O(x - x_c)^2, \quad y(x) = \frac{2c_M}{Q_2x_c^{5/2}}(x - x_c) + O(x - x_c)^2. \quad (45)$$

Since $f < 1$ and $y > 0$ this solution is only physical when the mass current $c_M < 0$ and then only for $x < x_c$, i.e., inside the critical point. The angle between the angular momentum current and the disc normal is θ where $\cos\theta = f$ so $\theta \sim (x_c - x)^{1/2}$ and the warp $\psi = x|d\hat{\mathbf{n}}/dx| \sim (x_c - x)^{-1/2}$. Thus the warp angle ψ is singular at the critical point.

The behavior of these solutions is consistent with the behavior seen in Fig. 6 at the critical obliquity: outside the critical radius, the disc is flat and the surface density decreases linearly to zero as the radius decreases to the critical radius (eq. 44), while inside the critical radius the azimuthal angle $\phi - \frac{1}{2}\pi$ of the warp normal varies as $(x_c - x)^{1/2}$, and the surface density decreases linearly to zero as the radius increases to the critical radius (eq. 45). Since the surface density is zero at the critical point, there is no viscous angular-momentum transport across it, only advective transport.

3 EVOLUTION OF VISCOUS DISCS WITH SELF-GRAVITY

Our treatment of accretion discs with self-gravity will be briefer and more approximate than the treatment of discs with a companion in the preceding section, for three main reasons: (i) AGN accretion discs are the only ones in which self-gravity is likely to be important, and these are less well-understood than accretion discs around stellar-mass BHs; (ii) the theory of bending waves in gas discs is remarkably sensitive to small deviations from Keplerian motion (cf. eq. 1); (iii) we found that warped steady-state accretion discs around a spinning BH with a companion do not exist for some values of the obliquity and viscosity, and this finding requires the best available disc models to be credible. In contrast we shall find that warped discs

with self-gravity exhibit interesting but physically plausible behavior even in relatively simple disc models, and there is no reason to believe that this behavior will change qualitatively in more sophisticated treatments.

We shall assume that the warp is small so that linearized theory can be used, and that the disc surface-density distribution is the same as in a flat disc. We shall also assume a simple model for the viscous damping of the warp.

We also ignore the effects of pressure in the disc. This assumption is problematic because Papaloizou & Lin (1995) showed that in gravitationally stable Keplerian discs ($Q > 1$ in eq. 69) the dispersion relation for bending waves is dominated by pressure rather than self-gravity. However, (i) this result depends sensitively on whether the disc is precisely Keplerian, and small additional effects such as centrifugal pressure support or relativistic apsidal precession can dramatically reduce the influence of pressure on the dispersion relation; (ii) modifying the Pringle–Ogilvie equations to include pressure is a difficult and unsolved problem.

The normal to the disc at radius r is $\hat{\mathbf{n}} = (n_x, n_y, n_z)$. We choose the axes so that the BH spin is along the positive z -axis; then since the warp is small $|n_x|, |n_y| \ll 1$. Write $\zeta(r, t) \equiv n_x + in_y$; then neglecting all terms quadratic in ζ the Lense–Thirring torque (3) causes precession of the angular momentum at a rate

$$\left. \frac{d\zeta}{dt}(r, t) \right|_{\text{LT}} = \frac{2(GM_\bullet)^2 a_\bullet}{c^3 r^3} i\zeta(r, t). \quad (46)$$

The equations of motion due to the self-gravity of the warped disc are given by classical Laplace–Lagrange theory (Murray & Dermott 1999),

$$\left. \frac{d\zeta}{dt}(r, t) \right|_{sg} = -\frac{i\pi G}{2(GM_\bullet r)^{1/2}} \int \frac{r' \Sigma(r') dr'}{\max(r, r')} \chi b_{3/2}^{(1)}(\chi) [\zeta(r, t) - \zeta(r', t)] \quad (47)$$

where $\Sigma(r)$ is the surface density, $\chi = \min(r, r')/\max(r, r')$ and the Laplace coefficient

$$b_{3/2}^{(1)}(\chi) = \frac{2}{\pi} \int_0^\pi \frac{\cos x dx}{(1 - 2\chi \cos x + \chi^2)^{3/2}} = \frac{4}{\pi\chi(1 - \chi^2)^2} [(1 + \chi^2)E(\chi) - (1 - \chi^2)K(\chi)] \quad (48)$$

with $K(\chi)$ and $E(\chi)$ complete elliptic integrals.

The equations of motion due to viscosity are derived by simplifying equations (24) and (25). The angular-momentum current proportional to $Q_1 \hat{\mathbf{n}}$ and the mass current C_M determine the steady-state surface density in a flat disc, which we assume to be given, so we drop these terms. The current proportional to Q_3 appears to play no essential role, so we drop this term as well. Furthermore we assume that the sound speed c_s is independent of radius (isothermal disc), and we replace Q_2 by $\frac{1}{2}\alpha_\perp$ (eq. 33). Thus we find

$$\left. \frac{d\zeta}{dt}(r, t) \right|_v = \frac{c_s^2 \alpha_\perp}{2(GM_\bullet r^3)^{1/2} \Sigma(r, t)} \frac{\partial}{\partial r} r^3 \Sigma(r, t) \frac{\partial \zeta}{\partial r}. \quad (49)$$

We now look for a steady-state solution in which $d\zeta/dt|_{LT+sg+v} = 0$. We replace the radius by the dimensionless variable $x = r/r_w$ where r_w is defined for a self-gravitating disc by equation (21), and we assume that the surface density is a power law, $\Sigma(r) = \Sigma_0/x^s$. The equations above simplify to

$$\frac{4}{x^{5/2}} \zeta - \int \frac{x'^{1-s} dx'}{\max(x, x')} \chi b_{3/2}^{(1)}(\chi) [\zeta(x) - \zeta(x')] - i\gamma \alpha_\perp x^{s-1} \frac{d}{dx} x^{3-s} \frac{d\zeta}{dx} = 0 \quad (50)$$

where γ is the viscosity parameter defined in equation (22). We impose the boundary conditions $d\zeta/dx = 0$ as $x \rightarrow 0$ and $x \rightarrow \infty$ (the disc is flat near the BH, and flat far outside the warp radius) and $\zeta \rightarrow \zeta_0$ at $x \rightarrow \infty$ (at large distances the normal to the disc is inclined to the spin axis of the BH by an angle $\theta = |\zeta_0| \ll 1$). Since equation (50) is linear, there is no loss of generality if we set $\zeta_0 = 1$.

In these dimensionless units, the shape of the warp is determined by only two parameters, the logarithmic slope of the surface-density distribution s , and the viscosity parameter $\gamma \alpha_\perp$. The relation between α and α_\perp is discussed after equation (33).

Fig. 8 shows the solutions of equation (50) for the surface-density slope $s = \frac{3}{5}$ appropriate for a gas-pressure dominated disc (eq. 66). The solid and dashed lines show the real and imaginary parts of $\zeta(x)$. For low-viscosity discs ($\gamma \alpha_\perp \ll 1$) we find that the disc develops bending waves inside the warp radius, and if the viscosity is sufficiently small the bending waves can grow in amplitude by orders of magnitude as the radius shrinks (the disappearance of the bending waves at $x < 0.18$ in the lower right panel is a numerical artifact, which arises because the wavelength of the bending waves becomes shorter than the resolution of the numerical grid, $\Delta \log_{10} x = 0.002$).

Many of the properties of the bending waves can be understood using a WKB analysis (Shu et al. 1983, hereafter SCL83). We shall quote the results from this paper without derivations. If we assume that the waves have the form $\zeta = A_\zeta(r) \exp[i\Phi(r)]$ with radial wavenumber $k \equiv d\Phi/dr$, then the dispersion relation is (SCL83 eq. 22, with $\omega = 0$ and $m = 1$)

$$|k| = \frac{2G^{3/2} M_\bullet^{5/2} a_\bullet}{\pi c^3 \Sigma(r) r^{9/2}}. \quad (51)$$

The WKB approximation is valid if the waves have short wavelengths, $|k|r \lesssim 1$, which in turn requires that the radius is less

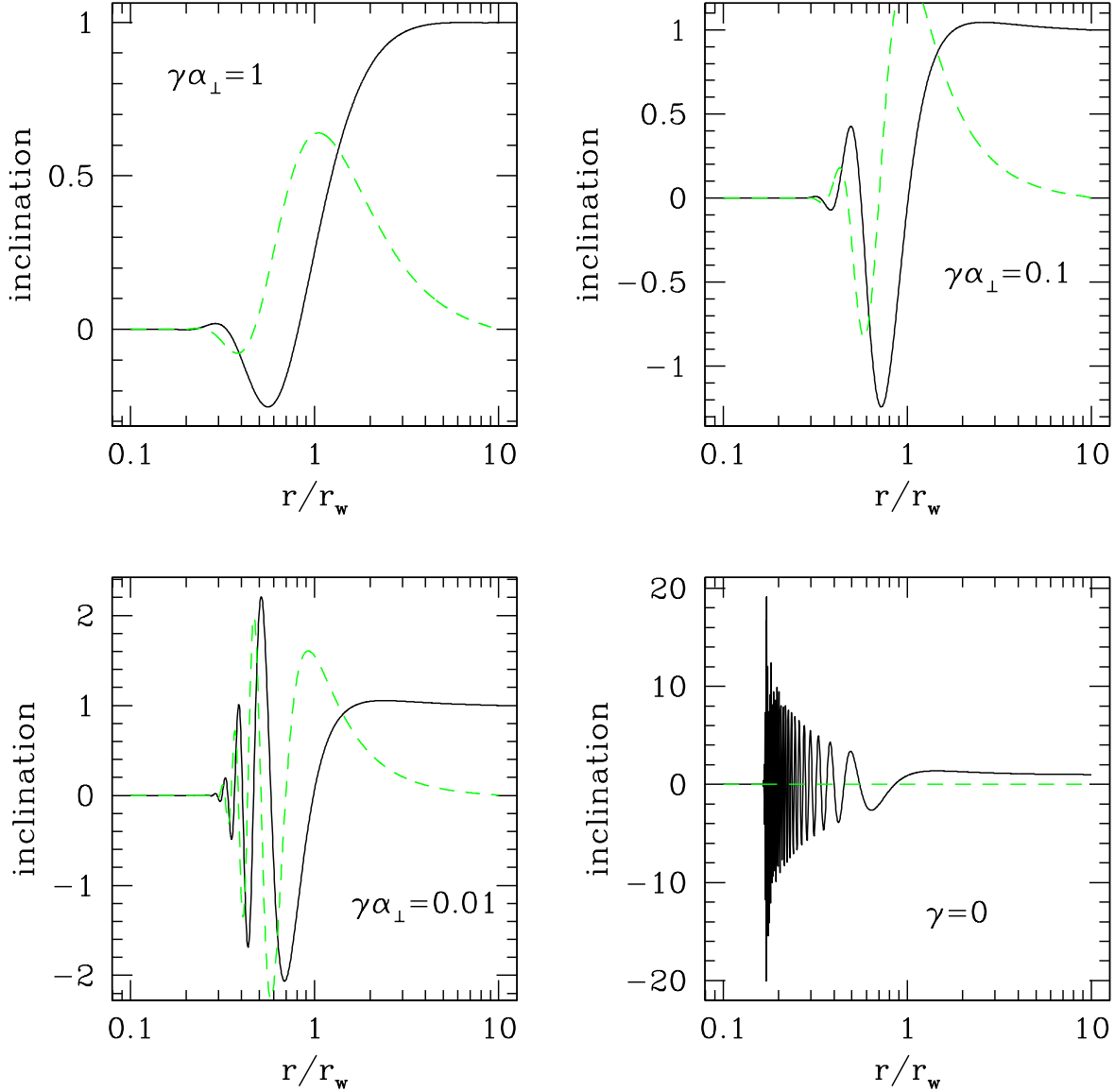


Figure 8. The steady-state shape of warped discs including Lense–Thirring torque, self-gravity, and viscosity (eq. 50). The four panels show four different values of the viscosity parameter $\gamma\alpha_{\perp}$ (eq. 22). The figures plot the real and imaginary parts of the complex inclination ζ (solid black and dashed green lines) as a function of the radius in units of the warp radius r_w (eq. 21). At large radii the disc is assumed to be flat with $\zeta = 1$; since eq. (50) is linear the results can be scaled to any (small) inclination. At small radii the disc is found to lie in the BH equator, $\zeta = 0$. Note the different vertical scales in the four panels. The disappearance of the oscillations at $x < 0.18$ in the lower right panel is a numerical artifact due to limited resolution.

than the warp radius r_w defined in equation (21); and this in turn requires that the dimensionless variable x in Fig. 8 is small compared to unity. For plausible variations of the surface density $\Sigma(r)$, the wavelength $2\pi/|k|$ gets shorter and shorter as the radius shrinks.

In the absence of viscosity, the maximum inclination of the bending wave varies as $A_{\zeta}(r) \propto [r^{3/2}\Sigma(r)]^{-1}$ (SCL83, eq. 34, with the inclination amplitude $A_{\zeta} = A(r)/r$) so if the surface density falls as r^{-s} then the amplitude of the warp grows as the radius shrinks whenever $s < \frac{3}{2}$, which is true for most disc models.

The waves are spiral, as may be deduced from the offset between the solid (real) and dashed (imaginary) curves in Fig. 8 (except in the lower right panel, where the viscosity is zero). The dispersion relation (51) does not distinguish leading and trailing waves but causality arguments do: trailing waves propagate inward (i.e. negative group velocity, see SCL83 eq. 23) while leading waves propagate outward. Waves excited by the warp in the outer part of the disc and damped at small radii by viscosity must propagate inward and hence are trailing.

In the case of low-viscosity Lense–Thirring discs that are warped because of a companion, we found that no solutions of

the Pringle–Ogilvie equations existed above a critical obliquity. These calculations suggest that self-gravitating discs are more well-behaved – that the long-range nature of the gravitational force allows a smooth transition from the outer to the inner orientation for any viscosity and obliquity, through the excitation of bending waves that are eventually damped by viscosity as they propagate inward. However, we caution that the analysis of this section is linear in the warp amplitude and it is possible that non-linear effects will prohibit a continuously varying warp shape once the obliquity is large enough.

This physical picture needs to be modified for AGN discs dominated by radiation pressure, where the surface density varies as $\Sigma(r) \propto r^{3/2}$ (eq. 65) out to a radius r_{pr} (eq. 68) where gas pressure begins to dominate, after which the surface density declines as $r^{-3/5}$. If $r_{pr} \lesssim r_w$, the bending waves are launched as usual at the warp radius r_w and propagate smoothly into the region $r < r_{pr}$, although their dispersion relation will change once they enter the radiation-dominated region. If r_{pr} is larger than r_w , the gravitational torque will include a significant contribution from material in the accretion disc near r_{pr} (the torque from material between $R \gg r$ and $2R$ varies as $G\Sigma(R)r^2/R \sim R^{1/2}$) in addition to the gravitational torque from local material. This extra torque will tend to counter-act the Lense–Thirring torque, and if it is large enough will prevent the excitation of bending waves.

In summary, for low-viscosity discs in which self-gravity is important, misalignment of the disc axis at large radii with the BH spin axis can excite bending waves inside the warp radius (21). For discs dominated by gas pressure, where the surface density $\Sigma(r) \propto r^{-0.6}$, Fig. 8 shows that the condition for exciting oscillatory waves is $\gamma\alpha_\perp \simeq 0.05$. For warps of sufficiently small amplitude, $\alpha_\perp = \frac{1}{2}\alpha^{-1}$ (eq. 33) so the condition for exciting bending waves is $\gamma \lesssim 0.01(\alpha/0.1)$.

4 RELATED WORK

Most treatments of warped Lense–Thirring discs neglect torques from the companion in determining the shape and evolution of the disc; we may call this the Bardeen–Petterson approximation since it first appears in Bardeen & Petterson (1975). The approximation is only valid if the torque associated with viscous angular-momentum transport exceeds the Lense–Thirring and companion torques at the point where the latter two are equal, the warp radius r_w (eq. 10), which in turn requires $\beta \gtrsim 1$ (eq. 30).

One of the few treatments of warped AGN accretion discs to include both Lense–Thirring and tidal torques is Martin et al. (2009). In fact the warp radius r_{warp} defined in their equation (15) is almost the same as the radius r_w defined in our equation (9), $r_{\text{warp}} = r_w/2^{2/9}$. Martin et al. also define a tidal radius r_{tid} and a Lense–Thirring radius r_{LT} where viscous torques balance tidal and Lense–Thirring torques, respectively. Our parameter β , defined in equation (30), is just $2^{1/9}(r_{\text{tid}}/r_{\text{LT}})^{10/9}$. Martin et al. find numerical solutions for steady-state discs with obliquities up to 80° but all their models have $r_{\text{tid}}/r_{\text{LT}} \geq 1$ and their models with obliquities $> 20^\circ$ have $r_{\text{tid}}/r_{\text{LT}} = 10$. Therefore they do not explore the regime with $\beta \lesssim 1$ where the critical obliquity becomes apparent.

Scheuer & Feiler (1996) give a simple analytic description of warped accretion discs, derived from the Pringle–Ogilvie equations by linearizing in the warp angle. The main focus of their analysis is on estimating the rate at which the BH aligns its angular momentum with that of the accreting material. Unfortunately, the linearization drops the term proportional to $|\partial\hat{\mathbf{n}}/\partial x|^2$ in equation (29), and without this term low-viscosity Lense–Thirring discs develop a thin boundary layer in which the warp angle jumps sharply, so the linearization is not self-consistent when β is sufficiently small.

Nixon & King (2012) and Nixon et al. (2012) have argued that warped discs described by the Pringle–Ogilvie equations can ‘break’ or ‘tear’ – divide into inner and outer parts with discontinuous orientations – if the obliquity $\gtrsim 45^\circ$. As described in their papers, this phenomenon does not appear to be directly related to our critical obliquity, for several reasons: (i) Nixon & King do not include torques from a companion in their analysis, i.e., the parameter β in equation (30) is very large, whereas we find that the critical obliquity is important only for $\beta \lesssim 1$ (Fig. 7). (ii) Nixon & King argue that the breaking phenomenon arises through the dependence of the viscosity parameters Q_i on the warp ψ , whereas we have found that the critical obliquity is almost the same whether or not this dependence is included in the differential equations. (iii) We do not see breaks in our high-viscosity ($\beta = 1000$) solutions, even for obliquities exceeding 88° , probably because our expression for $Q_2(\psi)$ is relatively flat (Fig. 2) whereas Nixon & King’s falls sharply toward zero for $\psi \gtrsim 1$ (their Fig. 1)⁴.

5 APPLICATION TO OBSERVED ACCRETION DISCS

The accreting BHs found in astrophysical systems span a wide range of inferred mass, from $M_\bullet \sim 5 M_\odot$ up to $\sim 10^{10} M_\odot$. Within this range they mostly fall – so far – into one of two distinct classes. At the low-mass end, $M_\bullet \sim 10 M_\odot$, the BHs all

⁴ The reason for this difference has been pointed out to us by G. Ogilvie (private communication). In a flat isothermal disc the sound speed and rms thickness are related by $c_s = H\Omega$; however, this relation no longer holds in a warped disc because a vertical oscillation is present, so hydrostatic equilibrium does not apply. Nixon & King’s ‘isothermal’ disc has H independent of the warp angle ψ whereas ours has c_s independent of ψ .

belong to close binary systems. The BH accretes mass from its companion star, either by Roche-lobe overflow or by capturing a fraction of the mass lost in a wind. Roche-lobe overflow tends to occur in low mass X-ray binaries (LMXBs), in which the companion is an evolved star with $M_\star \lesssim 1.5 M_\odot$. Wind-driven accretion is found in high mass X-ray binaries (HMXBs), where the companion is an O or B star with $M_\star \gtrsim 10 M_\odot$. The secondary star provides the tidal torque in equation (4), which is also thought to set the outer radius of the accretion disc. The dynamics and geometry of accretion in these systems is relatively well-understood and useful summaries are found in Frank et al. (2002) and Remillard & McClintock (2006).

The second class consists of supermassive BHs, with $M_\bullet \sim 10^5\text{--}10^{10} M_\odot$, which are found – so far – at the centres of galaxies and primarily accrete gas from the interstellar medium of their galaxy. When mass is supplied at sufficiently high rates, these are observed as AGN (Krolik 1999). The properties of these systems and how they are fed from the interstellar medium are less well understood than binary systems and there are fewer empirical constraints on the properties of the disc⁵.

We discuss these two classes of Lense–Thirring discs in the next two subsections.

5.1 Stellar-mass black holes in binary star systems

In these binaries the X-ray emission comes from the vicinity of a neutron star or BH (the ‘primary’), while the accreted mass and the tidal torque (4) comes from the companion star (the ‘secondary’). The masses of the primary and secondary, M and M_\star , and their orbital separation r_\star are inferred from the orbital period, the spectral type and velocity semi-amplitude of the secondary, periodic variations in the flux from the secondary due to its tidal distortion by the primary, eclipses, etc. In most cases the main evidence that the primary is a BH rather than a neutron star is that its mass exceeds the upper limit to the mass of a neutron star, $\sim 3 M_\odot$ (Lattimer & Prakash 2005).

Compilations of BH X-ray binary system parameters can be found in Tables 4.1 and 4.2 of McClintock & Remillard (2006) and Table 1 of Remillard & McClintock (2006). The inferred BH masses have a relatively narrow distribution – the best estimates in ~ 20 systems range from 4.5 to 14 M_\odot – with a mean near $M_\bullet \sim 7 M_\odot$. The BH spin a_\bullet is more difficult to measure. The two most commonly used methods are continuum fitting (e.g. McClintock et al. 2011) and Fe line modeling (Tanaka et al. 1995). Only a range of plausible spins can be inferred, even for the best systems, and both methods are subject to systematic uncertainties. For our purposes, the most important result is that the majority of systems are not consistent with $a_\bullet = 0$, implying that Lense–Thirring precession can be significant. Since the parameter β (eq. 30) depends relatively weakly on a_\bullet ($\beta \propto a_\bullet^{-4/9}$), we simply adopt $a_\bullet = 0.5$ as a characteristic value.

There is strong circumstantial evidence for warps in several X-ray binaries. The jets in the eclipsing X-ray binary SS 433 precess with a 162 d period, likely because the jet direction is normal to a precessing warped accretion disc. The 35 d period of Her X-1 is believed to be due to eclipses by a warped disc, and this is also the likely explanation for some of the long-term periodicities observed in other X-ray binaries, such as LMC X-4 and SMC X-1 (Charles et al. 2008). There is also evidence for misalignment between the binary orbital angular momentum and BH spin angular momentum in GRO J1655–40 and V4641 Sgr, if one assumes that the jet axis is aligned with the BH spin axis (e.g., Fragile et al. 2001; Maccarone 2002).

Most BH candidates with mass estimates are LMXBs, and only a handful are HMXBs. In the Roche-lobe overflow systems that comprise the bulk of LMXBs, it is thought that the tidal torque from the companion truncates the accretion disc at an outer radius $r_{\text{out}} \simeq 0.9 r_{L1}$ where r_{L1} is the Roche radius⁶ of the primary (Frank et al. 2002). Fitting of ellipsoidal variations of LMXBs with BH primaries generally yields r_{out} values consistent with this assumption (J. Orosz, private communication).

In LMXB systems, the secondaries are generally evolved F-K spectral types with $M_\star \sim M_\odot$, so we scale the companion mass M_\star to M_\odot . Orbital periods P range from a few hours to several days so we scale the period to $10^5 \text{ s} = 27.8 \text{ h}$. Then the separation or semimajor axis is

$$r_\star = \left(\frac{P}{2\pi}\right)^{2/3} [G(M_\bullet + M_\star)]^{1/3} = 9.3 R_\odot \left(\frac{P}{10^5 \text{ s}}\right)^{2/3} \left(\frac{M_\bullet + M_\star}{8 M_\odot}\right)^{1/3}. \quad (52)$$

The large range of P translates into a fairly broad range in r_\star . At the lower end of the range, corresponding to periods of a few hours, we expect $r_\star \simeq 2\text{--}3 R_\odot$, although r_\star can be much larger than this estimate in some cases such as GRS 1915+105: here $P = 804 \text{ h}$ so $r_\star = 87 R_\odot$ for $M_\bullet + M_\star = 8 M_\odot$.

For comparison, the warp radius (9) is

$$r_w = 0.19 R_\odot \left(\frac{a_\star}{0.5}\right)^{2/9} \left(\frac{M_\bullet}{7 M_\odot}\right)^{5/9} \left(\frac{M_\odot}{M_\star}\right)^{2/9} \left(\frac{r_\star}{10 R_\odot}\right)^{2/3}. \quad (53)$$

⁵ We do not consider the ultraluminous X-ray sources with $L \gtrsim 10^{40} \text{ erg s}^{-1}$. If these radiate isotropically and do not exceed the Eddington limit, they require BHs with $M_\bullet \gtrsim 100 M_\odot$. Whether or not these are, in fact, intermediate-mass BHs or normal HMXBs, the implied accretion rates suggest that ultraluminous X-ray sources arise from a short-lived phase of rapid mass transfer in a close binary (King et al. 2001).

⁶ ‘Roche radius’ is defined as the radius of a sphere with the same volume as the Roche lobe; the distance to the collinear Lagrange point from the centre of the star is larger by $\sim 25\text{--}40$ per cent, depending on the mass ratio. An analytic approximation to the Roche radius as a function of mass ratio is given by Eggleton (1983).

Assuming a mass ratio $M_\bullet/M_\star = 7$ the primary's Roche radius is $r_{L1} = 0.55r_\star$, so if the outer disc edge is at $r_{\text{out}} \simeq 0.9r_{L1}$ we have $r_{\text{out}} \simeq 0.5r_\star$. Hence, for typical LMXBs the warp radius (53) is well inside the outer disc radius (cf. eq. 52).

Similar conclusions hold for HMXBs. We consider the specific example of M33 X-7 since it is the best-understood HMXB system due to its X-ray eclipses and well-determined distance (Orosz et al. 2007; Liu et al. 2008). In this case we have $M_\star = 70 \pm 7 M_\odot$, $M_\bullet = 15.7 \pm 1.5 M_\odot$, $r_\star = 42 \pm 2 R_\odot$, $a_\bullet = 0.84 \pm 0.05$, yielding a warp radius $r_w = 0.34 R_\odot$. Orosz et al. also find that the outer radius of the disc is $r_{\text{out}} = (0.45 \pm 0.04)r_{L1}$; for the observed mass ratio $r_{L1} = 0.5r_\star$ (Eggleton 1983) so $r_{\text{out}} = 9.5 R_\odot$. Again, the warp radius is well inside the outer disc radius⁷.

The strength of the viscous torque can be parametrized through the disc aspect ratio H/r , which is related to the sound speed through $c_s = \Omega H$. The aspect ratio can be estimated using the standard thin-disc model of Shakura & Sunyaev (1973). In BH X-ray binaries, the warp radius is much larger than the BH event horizon, so we can ignore relativistic effects and corrections due to the inner boundary condition; moreover at the warp radius the radiation pressure is negligible. We can therefore use equation (66) below⁸ to estimate

$$\left(\frac{H}{r}\right)^2 \simeq 9.1 \times 10^{-5} \left(\frac{L}{0.01L_{\text{Edd}}}\frac{0.1}{\epsilon}\right)^{2/5} \left(\frac{0.1}{\alpha}\right)^{1/5} \left(\frac{7M_\odot}{M_\bullet}\right)^{3/10} \left(\frac{r}{R_\odot}\right)^{1/10}. \quad (54)$$

We assume that the Shakura–Sunyaev parameter α (eq. 26) is approximately 0.1, based on modeling of dwarf novae and soft X-ray transients (King et al. 2007).

This equation is determined by balancing local viscous heating with radiative cooling. However, the spectra from the outer regions of discs in LMXBs show evidence that irradiation by X-rays dominates over local dissipation (van Paradijs & McClintock 1994). Simple models of the X-ray irradiated outer disc imply only a weak dependence of H/R on R (e.g., Dubus et al. 1999). So we make an alternative estimate of the aspect ratio, valid for the outer parts of the disc, by scaling to a characteristic temperature T and assuming hydrostatic equilibrium. Then we have approximately

$$\left(\frac{H}{r}\right)^2 \simeq \frac{kTr}{GM_\bullet m_p} \simeq 2 \times 10^{-4} \frac{r}{3R_\odot} \frac{7M_\odot}{M_\bullet} \frac{T}{10^4 \text{ K}}. \quad (55)$$

Soft X-ray transient LMXBs are believed to be triggered by a disc instability associated with hydrogen ionization (Lasota 2001) so one expects the outer disc has $T \lesssim 10^4$ K at the beginning of an outburst, but the temperature may rise to as high as $T \sim 10^5$ K during outburst.

Taken together equations (54) and (55) imply $(H/R)^2 \simeq 10^{-5} - 10^{-3}$ in most discs. Inserting the above estimates into equation (30) we find

$$\beta = 120 \left(\frac{0.5}{a_\bullet}\right)^{2/3} \left(\frac{M_\odot}{M_\star}\right)^{1/3} \left(\frac{7M_\odot}{M_\bullet}\right)^{2/3} \frac{r_\star}{10R_\odot} \frac{(H/r)^2}{10^{-4}} \quad (56)$$

where H/r is evaluated at the warp radius.

Therefore, we generally expect $\beta \gg 1$, that is, viscous torques are more important than the torque from the secondary star in determining the warp shape. In order to have the companion torque dominate the warp dynamics, we need $\alpha_\perp \beta \lesssim 1$, which requires a nearby companion (the shortest orbital periods of X-ray binaries are a few hours, corresponding to $r_\star \sim 3 R_\odot$) and, more importantly, a cool disc with $H/r \lesssim 10^{-3}$. This is plausible for quiescent discs, with low accretion rates, as long as irradiation by the central X-ray source does not enforce a larger H/r at the radius of the warp. One might even speculate that the absence of a steady-state solution for warped discs with $\beta \lesssim 1$ is the process that drives disc instability and outbursts in some X-ray binaries.

5.2 Warped discs in active galactic nuclei

There is strong circumstantial evidence that warps are common in AGN accretion discs. Maser discs having modest warps on 0.1–1 pc scales are present in NGC 4258 (Herrnstein et al. 2005), Circinus (Greenhill et al. 2003), and four of the seven galaxies examined by Kuo et al. (2011). Warped discs may obscure some AGN and thus play a role in unification models of AGN based on orientation (Nayakshin 2005). The angular-momentum axis of material accreting onto the AGN, as traced by jets or other indicators, is not aligned with the axis of the host galaxy on large scales (Kinney et al. 2000). Radio jets from AGN often show wiggles or bends that may arise from precession of the jet source (e.g., 3C 31). Finally, frequent and variable misalignments of the BH spin axis with the angular momentum of accreted gas are expected theoretically because of clumpy gas accretion, inspiral of additional BHs, and rapid angular-momentum transport within gravitationally unstable gas discs (Hopkins et al. 2012).

⁷ Note that the common assumption that $r_{\text{out}} = 0.9r_{L1}$ is not confirmed in M33 X-7, where the eclipse models give a result a factor of two smaller. In wind-fed HMXBs the disc could plausibly be truncated at smaller radii via interactions with the wind. Direct constraints on r_{out} in other HMXBs are hampered by the dominance of the secondary in the optical band (see e.g. Orosz et al. 2009).

⁸ Equation 2.16 of Shakura & Sunyaev 1973 gives the same result to within 30 per cent for their assumed efficiency $\epsilon = 0.06$.

AGN accretion discs are much less well-understood than X-ray binary discs. There is no obvious source of external torque analogous to the companion star in X-ray binaries – except in the case of binary BHs, which we defer to §5.2.1. In the absence of external torques, warping can arise from a misalignment between the orbital angular momentum of the inflowing material at the outer edge of the disc and the spin angular momentum of the BH at its centre. Then in the absence of other torques the shape of the warp is determined by the competition between viscous torques and the Lense–Thirring torque (the Bardeen–Petterson approximation).

However, AGN discs are much more massive than X-ray binary discs relative to their host BH, and this raises the possibility that the self-gravity of AGN discs plays a prominent role in determining the shape of the disc.

Self-gravitating⁹ warped discs have mostly been investigated in the context of galaxy discs, which are sometimes warped in their outer parts. There is a large literature on the dynamics of galactic warps (e.g., Hunter & Toomre 1969; Sparke & Casertano 1988; Binney 1992; Nelson & Tremaine 1996; Sellwood 2013). Very few authors have examined the properties of self-gravitating warped discs in the context of AGN. One notable exception is Ulubay-Siddiki et al. (2009), who computed the shapes of warped self-gravitating discs orbiting a central mass, modeling the disc as a set of concentric circular rings and computing the gravitational torques between each ring pair. However, they did not include either Lense–Thirring or viscous torques so their calculations do not address the issues that are the focus of the present paper.

We first describe a simple analytic model for flat AGN accretion discs, which we shall use to estimate the relative importance of self-gravity and viscous stresses in warped discs. Our model is similar to earlier analytic models by Shakura & Sunyaev (1973), Pringle (1981), Collin-Souffrin & Dumont (1990), and others.

We assume that the density $\rho(r, z)$ in the disc is small compared to M_\bullet/r^3 . Then hydrostatic equilibrium requires

$$\frac{dp_t}{dz} = \Omega^2 \mathfrak{R}_z \rho z, \quad (57)$$

where $p_t = p_g + p_r$ is the sum of the gas and radiation pressure, $\Omega^2 = GM_\bullet/r^3$, and \mathfrak{R}_z is a dimensionless factor discussed below. The equation of energy conservation is

$$F_r = \frac{3}{4} \Omega \frac{\mathfrak{R}_R}{\mathfrak{R}_T} \int dz \tau_{r\phi}, \quad (58)$$

where F_r is the emissivity from one surface of the disc and $\tau_{r\phi}$ is the viscous stress tensor. Together with \mathfrak{R}_z above, \mathfrak{R}_R and \mathfrak{R}_T are dimensionless factors that depend on radius and the BH spin parameter a_\bullet and approach unity for $r \gg R_g$, where as usual $R_g = GM_\bullet/c^2$ is the gravitational radius of the BH. These quantities, defined in Chapter 7 of Krolik (1999), account approximately for general-relativistic effects and incorporate the assumption of no torque at the radius r_{ISCO} of the innermost stable circular orbit.

Coupling equation (58) to the equation for conservation of angular momentum in a flat steady-state disc allows one to solve for F_r ,

$$F_r = \frac{3c^3(L/L_{\text{Edd}})}{2\kappa R_g \epsilon (r/R_g)^3} \mathfrak{R}_R, \quad (59)$$

where L/L_{Edd} is the ratio of the bolometric luminosity of the disc to the Eddington luminosity, κ is the electron scattering opacity (assumed to be $\simeq 0.34 \text{ cm}^2 \text{ g}^{-1}$), and $\epsilon = L/(M_\bullet c^2)$ is the radiative efficiency.

We now make the standard α -disc approximations that the stress has the form (eq. 26)

$$\tau_{r\phi} = -\eta r \frac{d\Omega}{dr} = \frac{3}{2} \alpha p_t, \quad (60)$$

and that the rate of energy dissipation per unit mass is independent of z . Then the radiation pressure and the temperature at the midplane of the disc are

$$p_{r0} = \frac{F_r \kappa \Sigma}{4c}, \quad T_0 = \left(\frac{3F_r \kappa}{16\sigma_B} \right)^{1/4}, \quad (61)$$

where σ_B is the Stefan-Boltzmann constant. The gas pressure at the midplane is

$$p_{g0} = \frac{\rho_0 k_B T_0}{\mu} = \frac{\rho_0 k_B}{\mu} \left(\frac{3F_r \kappa}{16\sigma_B} \right)^{1/4} = \left(\frac{3F_r \kappa}{16\sigma_B} \right)^{1/4} \frac{k_B}{\mu} \frac{\Sigma^{5/4}}{2H}, \quad (62)$$

where k_B and ρ_0 are Boltzmann's constant and the midplane density. The mean particle mass μ is taken to be the proton mass times 0.62, appropriate for fully ionized hydrogen plus 30 per cent helium by mass. In the last equation we have replaced ρ_0 by $\Sigma/(2H)$ where H is the disc thickness.

We now substitute these results into equations (57) and (58) with the replacements $d/dz \rightarrow 1/H$, $z \rightarrow H$, and $\int dz \rightarrow 2H$,

⁹ As described in the Introduction, by ‘self-gravitating’ we mean that the self-gravity of the warped disc dominates the angular-momentum precession rate, not that the disc is gravitationally unstable or that its mass is comparable to the BH mass.

to obtain

$$\frac{F_r \kappa \Sigma}{4c} + \left(\frac{3F_r \kappa}{16\sigma_B} \right)^{1/4} \frac{k_B \Sigma^{5/4}}{\mu} - \frac{\Omega^2 \mathfrak{R}_z H \Sigma}{2} = 0 \quad (63)$$

and

$$\frac{H F_r \kappa \Sigma}{4c} + \left(\frac{3F_r \kappa}{16\sigma_B} \right)^{1/4} \frac{k_B \Sigma^{5/4}}{2\mu} - \frac{4F_r \mathfrak{R}_T}{9\Omega \alpha \mathfrak{R}_R} = 0. \quad (64)$$

For given values of the radius r , the gravitational radius R_g , the efficiency ϵ , and the Eddington ratio L/L_{Edd} , the second of these equations can be solved for the disc thickness H . Then the result can be substituted into the first equation to yield a tenth degree polynomial in $\Sigma^{1/4}$, which can be solved numerically to find the surface density (Zhu et al. 2012).

The analysis is simpler when the accretion disc is dominated by radiation pressure or gas pressure. For radiation-pressure dominated discs we set $p_g = 0$ in equations (63) and (64). We then find

$$\begin{aligned} \Sigma_r &= \frac{2^6}{3^3} \frac{\mathfrak{R}_z \mathfrak{R}_T}{\mathfrak{R}_R^2} \frac{\epsilon}{\alpha \kappa} \frac{L_{\text{Edd}}}{L} \left(\frac{r}{R_g} \right)^{3/2} = 70 \text{ g cm}^{-2} \frac{\mathfrak{R}_z \mathfrak{R}_T}{\mathfrak{R}_R^2} \frac{\epsilon}{0.1} \frac{0.1}{\alpha} \frac{0.1 L_{\text{Edd}}}{L} \left(\frac{r}{R_g} \right)^{3/2} \\ H_r &= \frac{3 \mathfrak{R}_R}{4 \mathfrak{R}_z} \frac{L}{L_{\text{Edd}}} \frac{R_g}{\epsilon} = 1.1 \times 10^{13} \text{ cm} \frac{\mathfrak{R}_R}{\mathfrak{R}_z} \frac{0.1}{\epsilon} \frac{L}{0.1 L_{\text{Edd}}} \frac{M_\bullet}{10^8 M_\odot}. \end{aligned} \quad (65)$$

Similarly, when radiation pressure is negligible,

$$\begin{aligned} \Sigma_g &= \frac{2^{14/5} \pi}{3^{7/5} 5^{1/5}} \frac{\mu^{4/5} (GM_\bullet c)^{1/5}}{\kappa^{4/5} h^{3/5} \alpha^{4/5} \epsilon^{3/5}} \frac{\mathfrak{R}_T^{4/5}}{\mathfrak{R}_R^{1/5}} \left(\frac{L}{L_{\text{Edd}}} \frac{R_g}{r} \right)^{3/5} \\ &= 1.4 \times 10^7 \text{ g cm}^{-2} \frac{\mathfrak{R}_T^{4/5}}{\mathfrak{R}_R^{1/5}} \left(\frac{0.1}{\alpha} \right)^{4/5} \left(\frac{M_\bullet}{10^8 M_\odot} \right)^{1/5} \left(\frac{0.1}{\epsilon} \frac{L}{0.1 L_{\text{Edd}}} \frac{R_g}{r} \right)^{3/5} \end{aligned} \quad (66)$$

and

$$\begin{aligned} H_g &= \frac{3^{1/5} 5^{1/10}}{2^{2/5} \pi^{1/2}} \frac{h^{3/10} (GM_\bullet)^{9/10}}{\mu^{2/5} \kappa^{1/10} c^{21/10} \alpha^{1/10} \epsilon^{1/5}} \frac{\mathfrak{R}_R^{1/10} \mathfrak{R}_T^{1/10}}{\mathfrak{R}_z^{1/2}} \left(\frac{L}{L_{\text{Edd}}} \right)^{1/5} \left(\frac{r}{R_g} \right)^{21/20} \\ &= 2.5 \times 10^{10} \text{ cm} \frac{\mathfrak{R}_R^{1/10} \mathfrak{R}_T^{1/10}}{\mathfrak{R}_z^{1/2}} \left(\frac{0.1}{\alpha} \right)^{1/10} \left(\frac{M_\bullet}{10^8 M_\odot} \right)^{9/10} \left(\frac{0.1}{\epsilon} \right)^{1/5} \left(\frac{L}{0.1 L_{\text{Edd}}} \right)^{1/5} \left(\frac{r}{R_g} \right)^{21/20}. \end{aligned} \quad (67)$$

With these scalings, we can compute most properties of interest in the disc. For example, radiation pressure dominates when $H_r > H_g$ which occurs for radii less than

$$r_{pr} \simeq 5.0 \times 10^{15} \text{ cm} \left(\frac{\alpha}{0.1} \right)^{2/21} \left(\frac{0.1}{\epsilon} \frac{L}{0.1 L_{\text{Edd}}} \right)^{16/21} \left(\frac{M_\bullet}{10^8 M_\odot} \right)^{23/21} \frac{\mathfrak{R}_R^{6/7}}{\mathfrak{R}_z^{10/21} \mathfrak{R}_T^{2/21}} \Big|_{r_{pr}}. \quad (68)$$

The disc is gravitationally unstable if Toomre's (1964) Q parameter is less than unity; this parameter is approximately

$$Q = \frac{\Omega^2 H}{\pi G \Sigma}. \quad (69)$$

In the radiation- and gas-pressure dominated regimes (respectively) we have

$$\begin{aligned} Q_r &= 3.1 \times 10^{12} \frac{\mathfrak{R}_R^3}{\mathfrak{R}_z^2 \mathfrak{R}_T} \left(\frac{L}{0.1 L_{\text{Edd}}} \frac{0.1}{\epsilon} \right)^2 \frac{10^8 M_\odot}{M_\bullet} \frac{\alpha}{0.1} \left(\frac{R_g}{r} \right)^{9/2} \\ Q_g &= 3.5 \times 10^4 \frac{\mathfrak{R}_R^{3/10}}{\mathfrak{R}_T^{7/10} \mathfrak{R}_z^{1/2}} \left(\frac{0.1 L_{\text{Edd}}}{L} \frac{\epsilon}{0.1} \right)^{2/5} \left(\frac{10^8 M_\odot}{M_\bullet} \right)^{13/10} \left(\frac{\alpha}{0.1} \right)^{7/10} \left(\frac{R_g}{r} \right)^{27/20}. \end{aligned} \quad (70)$$

Similarly, we can compute the warp radius (eq. 21)

$$\begin{aligned} r_{w,r} &= 4.3 \times 10^{15} \text{ cm} \left(\frac{a_\bullet}{0.5} \right)^{1/5} \left(\frac{\alpha}{0.1} \frac{0.1}{\epsilon} \frac{L}{0.1 L_{\text{Edd}}} \right)^{1/5} \left(\frac{M_\bullet}{10^8 M_\odot} \right)^{4/5} \frac{\mathfrak{R}_R^{2/5}}{\mathfrak{R}_T^{1/5} \mathfrak{R}_z^{1/5}} \Big|_{r_{w,r}} \\ r_{w,g} &= 3.9 \times 10^{15} \text{ cm} \left(\frac{a_\bullet}{0.5} \right)^{10/29} \left(\frac{\alpha}{0.1} \right)^{8/29} \left(\frac{\epsilon}{0.1} \right)^{6/29} \left(\frac{0.1 L_{\text{Edd}}}{L} \right)^{6/29} \left(\frac{M_\bullet}{10^8 M_\odot} \right)^{17/29} \frac{\mathfrak{R}_R^{2/29}}{\mathfrak{R}_T^{8/29}} \Big|_{r_{w,g}}. \end{aligned} \quad (71)$$

Equation (71) gives implicit relations for r_w because of the radial dependence of the relativistic factors. However, this dependence is rather weak for typical AGN disc models: for the case $a_\bullet = 0.5$, $M = 10^8 M_\odot$, $\alpha = 0.1$ and $L/L_{\text{Edd}} = 0.1$, we have $\mathfrak{R}_R = 0.81$, $\mathfrak{R}_T = 0.81$, and $\mathfrak{R}_z = 1.01$ at r_w , corresponding to values of 0.96 and 1.05 for the products of relativistic factors in the radiation-pressure and gas-pressure dominated limits of equation (71).

The characteristic ratio of the viscous and self-gravity torques is (cf. eq. 22)

$$\begin{aligned}
\gamma &= \frac{c_s^2}{\pi G \Sigma r} \Big|_{r_w} = \frac{H^2 \Omega^2}{\pi G \Sigma r} \Big|_{r_w} \\
&= 0.14 \left(\frac{0.5}{a_\bullet} \right)^{11/10} \left(\frac{0.1}{\alpha} \right)^{1/10} \left(\frac{0.1}{\epsilon} \frac{L}{0.1 L_{\text{Edd}}} \right)^{19/10} \left(\frac{M_\bullet}{10^8 M_\odot} \right)^{1/10} \frac{\mathfrak{R}_R^{9/5} \mathfrak{R}_T^{1/10}}{\mathfrak{R}_z^{19/10}} \Big|_{r_w, r} \\
&= 0.056 \left(\frac{0.5}{a_\bullet} \right)^{13/29} \left(\frac{\alpha}{0.1} \right)^{7/29} \left(\frac{0.1}{\epsilon} \frac{L}{0.1 L_{\text{Edd}}} \right)^{2/29} \left(\frac{10^8 M_\odot}{M_\bullet} \right)^{25/29} \frac{\mathfrak{R}_R^{9/29}}{\mathfrak{R}_T^{7/29} \mathfrak{R}_z} \Big|_{r_w, g}
\end{aligned} \tag{72}$$

where as usual the two equations correspond to the radiation-pressure dominated and the gas-pressure dominated regions.

Thus, in our fiducial case – a disc surrounding a $10^8 M_\odot$ BH radiating at 10 per cent of the Eddington luminosity, with spin parameter $a_\bullet = 0.5$, efficiency $\epsilon = 0.1$, and Shakura–Sunyaev parameter $\alpha = 0.1$ – the gravitational radius is $R_g = 1.48 \times 10^{13}$ cm; the warp radius is just inside the radiation-pressure dominated region at $r_w = 4.3 \times 10^{15}$ cm $= 290 R_g$; the disc becomes gas-pressure dominated outside $r_{pr} = 5.0 \times 10^{15}$ cm $\simeq 340 R_g$; the disc becomes gravitationally unstable outside 3.4×10^{16} cm $\simeq 2300 R_g$; and the disc warp is governed by Lense–Thirring and self-gravitational torques, with viscous torques smaller by a factor of $\gamma \alpha_\perp \simeq 0.14 \alpha_\perp$ where $\alpha_\perp \sim 1$ for a Shakura–Sunyaev parameter $\alpha \simeq 0.1$.

We supplement these formula with three sets of plots. These plots are based on the analysis in equations (57)–(64) with three refinements to the analytic formulae (65)–(72): (i) we include both gas and radiation pressure at all radii; (ii) we include the effects of the relativistic parameters \mathfrak{R}_z , \mathfrak{R}_T , and \mathfrak{R}_R ; (iii) we compute the efficiency ϵ from the spin parameter a_\bullet using the estimates from Novikov & Thorne (1973). Thus the plots assume thin-disc accretion with no torque at the inner boundary, which is assumed to lie at r_{ISCO} , the radius of the innermost stable circular orbit.

Fig. 9 shows Toomre’s Q (eq. 69), the aspect ratio H/r , the surface density Σ , and the ratio γ of viscous and self-gravity torques for BH masses of $10^7 M_\odot$, $10^8 M_\odot$, and $10^9 M_\odot$. Fig. 10 shows a similar plot for Eddington ratios L/L_{Edd} of 1, 0.1, and 0.01. Figs. 9 and 10 show that the transition from radiation pressure to gas pressure dominance occurs in the range of 100 to $10^4 R_g$, and depends more strongly on L/L_{Edd} than M_\bullet . The radii where Q declines below unity (onset of local gravitational instability) and γ declines below unity (self-gravity torque stronger than viscous torque) are not very different, so care must be taken when applying analytic formulae that assume either radiation or gas pressure to dominate.

Fig. 11 compares the warp radius r_w to three characteristic disc radii for a range of disc parameters. We have defined the self-gravity radius r_Q as the radius where $Q = 1$, r_{pr} as the radius where the gas and radiation pressure are equal (cf. eq. 68), and r_{5000} as the half-light radius for emission at 5000 Å, assuming that the disc radiates locally as a blackbody. Since γ is smaller than Q by a factor of H/r (see discussion following eq. 22), we always have $r_w < r_Q$. The disc is generally in the radiation-dominated regime at r_w , but can fall in the gas-pressure dominated region for smaller BH mass M_\bullet , smaller Eddington ratio L/L_{Edd} , or spin parameter a_\bullet near unity. The dependence of all the characteristic radii on a_\bullet is rather weak, except for $a_\bullet \rightarrow 0$ or 1.

Note that for $\alpha \simeq 0.1$ all of the discs shown in these figures have $\alpha \gg H/r$ (except for $r \lesssim 100 R_g$ when $L/L_{\text{Edd}} = 1$) so the condition (1) for non-resonant warp behavior is satisfied by a large margin.

For most of the parameter space we have examined the warp radius r_w is just outside (1–3 times larger than) the optical radius r_{5000} . However, if warping causes the disc to intercept a larger fraction of the emission from smaller radii the region where the warp is strong may dominate the optical emission. The flux of radiation coming from the inner disc that irradiates the outer disc is approximately

$$F_{\text{irr}} \approx \frac{L_{\text{in}}}{4\pi r^2} \cos \theta \tag{73}$$

where L_{in} is the characteristic luminosity from the inner disc and θ is the angle between the normal to the warped outer disc and the incoming flux. For thin discs, $\cos \theta \simeq H/r \ll 1$ and, since H is independent of r in the radiation-dominated regime, $F_{\text{irr}} \propto r^{-3}$. This is the same scaling as the intrinsic disc emission (eq. 59) so disc irradiation has little effect on the radial emission profile of an unwarped disc. However, if the disc has a significant warp, $\cos \theta \gg H/r$ and the irradiating flux can exceed the intrinsic disc emission. In this case the characteristic disc temperature will be

$$T_{\text{irr}} \approx \left(\frac{\chi L}{\pi \sigma_B r_{w,r}^2} \right)^{1/4} \approx 1.1 \times 10^4 \text{ K} \left(\frac{\chi}{0.01} \right)^{1/4} \left(\frac{0.5}{a_\bullet} \frac{0.1}{\alpha} \frac{\epsilon}{0.1} \right)^{1/10} \left(\frac{L}{L_{\text{Edd}}} \right)^{3/20} \left(\frac{10^8 M_\odot}{M_\bullet} \right)^{3/20}, \tag{74}$$

where χ is a (poorly constrained) reduction factor added to account for the fraction of the disc luminosity intercepted by the warp, the characteristic emitting area of the warp, and the albedo. The wavelength at which blackbody emission peaks for $T_{\text{irr}} = 1.1 \times 10^4$ K is $\lambda \simeq hc/3k_B T_{\text{irr}} = 4400 \text{ Å}$. Since r_w exceeds the the nominal half-light radius of the unirradiated disc, the reradiated emission at the warp can easily dominate. If so, the true half-light radius for optical emission should be roughly given by r_w rather than r_{5000} .

This result is relevant to recent constraints on the size of quasar emission regions obtained by modeling the variability due to gravitational microlensing in an intervening galaxy. In the majority of cases that have been studied, the sizes inferred

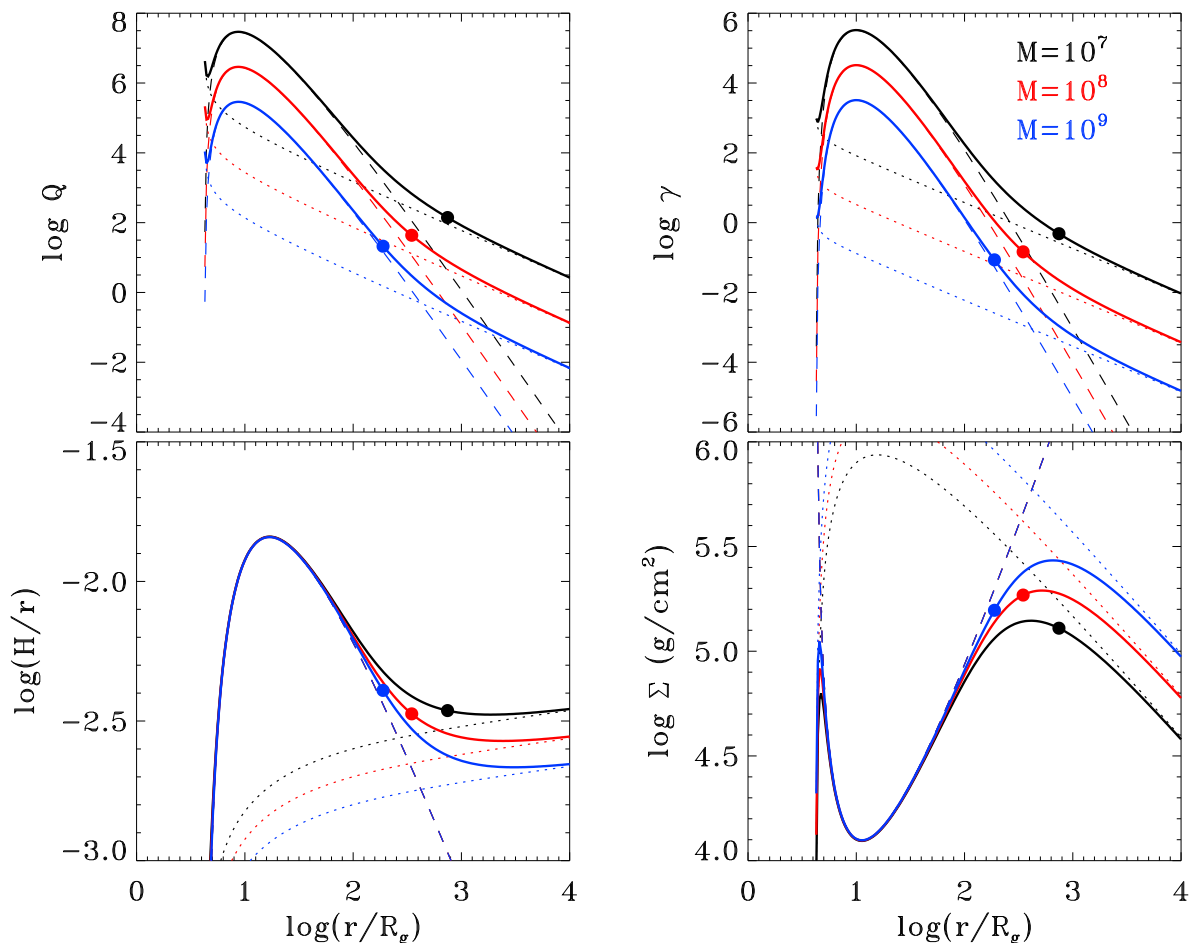


Figure 9. Properties of AGN accretion discs with $\alpha = 0.1$, $a_\bullet = 0.5$, $L/L_{\text{Edd}} = 0.1$, and BH masses $10^7 M_\odot$ (black), $10^8 M_\odot$ (red), and $10^9 M_\odot$ (blue). The plots show Toomre’s Q parameter (top left panel), the ratio γ (eq. 22) of self-gravity to viscous torque (top right), the aspect ratio H/r (bottom left) and the surface density (bottom right) versus radius in units of the gravitational radius $R_g = GM_\bullet/c^2$. The solid curves are computed via direct numerical solution of equations (63) and (64), while the dashed and dotted curves show the analytic approximations assuming that radiation and gas pressure (respectively) dominate. The warp radii are marked by filled circles.

from microlensing exceed the predicted half-light radii of flat α -disc models by factors of ~ 3 – 10 (e.g. Mortonson et al. 2005; Pooley et al. 2007). Morgan et al. (2010) find a best fit in which the microlensing size at 2500\AA scales as $M_\bullet^{0.8}$ for a sample of 11 sources with estimated $M_\bullet = 4 \times 10^7 M_\odot$ – $2.4 \times 10^9 M_\odot$. This is the same scaling as $r_{w,r}$ with M_\bullet in equation (71) and also agrees well with the dependence of the warp radius on M_\bullet found in Fig. 11. Unfortunately this is not a very sensitive test: for a flat disc, the radius at a given temperature scales as $M_\bullet^{2/3}$, and in the Bardeen–Peterson approximation the warp radius scales as $M_\bullet^{9/8}$. The absolute scale for the microlensing size at 2500\AA is a factor of ~ 6 smaller than our estimate for $r_{w,r}$, but this is subject to some uncertainty and might be accounted for by bending waves excited interior to r_w (compare Fig. 8).

An important but poorly understood issue is what fraction of AGN accretion discs are likely to be warped. Over long times, warps are damped out as the BH spin axis aligns with the outer disc. A rough estimate of this time-scale is $t_{\text{align}} \simeq L_\bullet / (\pi r^2 \Sigma T_{\text{LT}})_{r_w}$ where L_\bullet is the spin angular momentum of the BH and the quantity in parentheses is the Lense–Thirring torque per unit mass T_{LT} times the disc mass evaluated at the warp radius r_w . Using equation (3) and the expression for L_\bullet given just above it, we find

$$t_{\text{align}} \simeq \frac{M_\bullet}{2\pi c R_g^{3/2}} \left(\frac{r^{1/2}}{\Sigma} \right)_{r_w} = \frac{r_w^4}{2ca_\bullet R_g^3}. \quad (75)$$

where in the second expression we have used (21) to eliminate the surface density. For our fiducial case – $M_\bullet = 10^8 M_\odot$, $L = 0.1L_{\text{Edd}}$, $a_\bullet = 0.5$, $\epsilon = 0.1$, $\alpha = 0.1$ – the warp radius is $\sim 300R_g$ and $t_{\text{align}} = 1.3 \times 10^5 \text{ yr} (r_w/300R_g)^4$, much shorter than the typical AGN lifetime (the Salpeter time, $5 \times 10^7 \text{ yr}$ for $\epsilon = 0.1$). Much more uncertain is the time-scale on which warps are excited. High-resolution simulations of the centres of galaxies show order unity variations in the gas inflow rate at

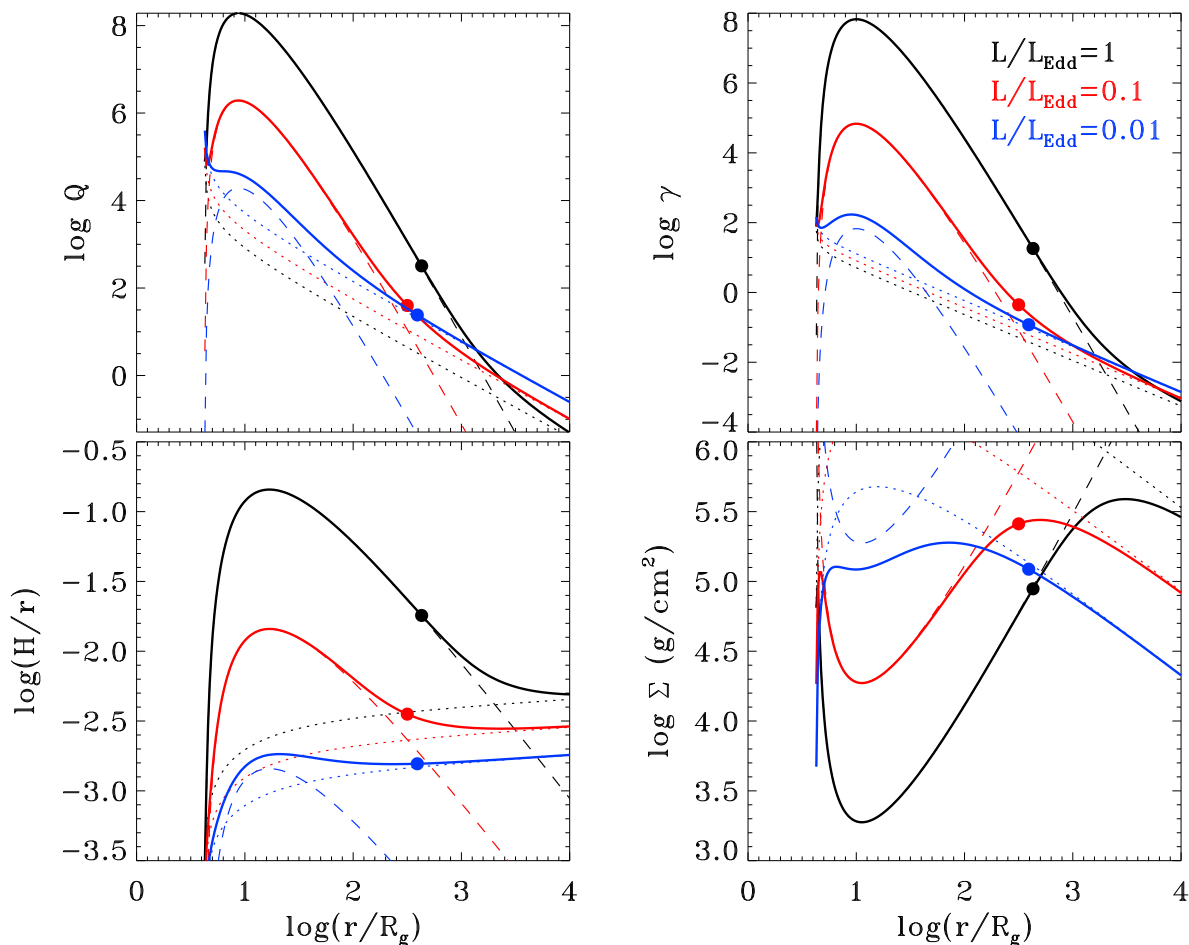


Figure 10. As in Fig. 9, except for BH mass $10^8 M_\odot$ and Eddington ratios of 1 (black), 0.1 (red), and 0.01 (blue).

0.1 pc on time-scales less than 10^5 yr (Hopkins & Quataert 2010, fig. 6) and these are presumably accompanied by similar variations in the angular momentum of the inflowing gas. In such an environment the orientation of the outer parts of the accretion disc is likely to vary stochastically on time-scales less than the damping time, and this case most AGN accretion discs will be warped.

5.2.1 Binary black holes

Most galaxies contain supermassive BHs at their centres, and when galaxies merge these BHs will spiral to within a few parsecs of the centre of the merged galaxy through dynamical friction (e.g., Begelman et al. 1980; Yu 2002). Whether they continue to spiral to smaller radii remains unclear, but if the binary decays to a sufficiently small semimajor axis – typically 0.1–0.001 pc, depending on the galaxy and the BH mass ratio – the loss of orbital energy through gravitational radiation will ensure that they merge. If one of the BHs (the primary) supports an accretion disc, and the spin axis of the primary is misaligned with the orbital axis of the binary, the accretion disc will be warped¹⁰. In this case both the self-gravity of the disc and the tidal field from the secondary, as well as viscous stresses and the Lense–Thirring effect, can play important roles in shaping the warp. For the sake of simplicity, we do not examine all of these torques simultaneously: here we first consider an AGN accretion disc without self-gravity orbiting one member of a binary BH, then compare the strength of the torques and the characteristic warp radius to those in an accretion disc with self-gravity orbiting an isolated BH.

Let M_\bullet be the mass of the primary and μM_\bullet the mass of the other BH (the secondary). We assume for simplicity that the orbit is circular, with semimajor axis r_* . The time required for the two BHs to merge due to gravitational radiation is

¹⁰ There can also be a circumbinary accretion disc, which may also be warped, but the structure of such discs is poorly understood and we will not discuss them here.

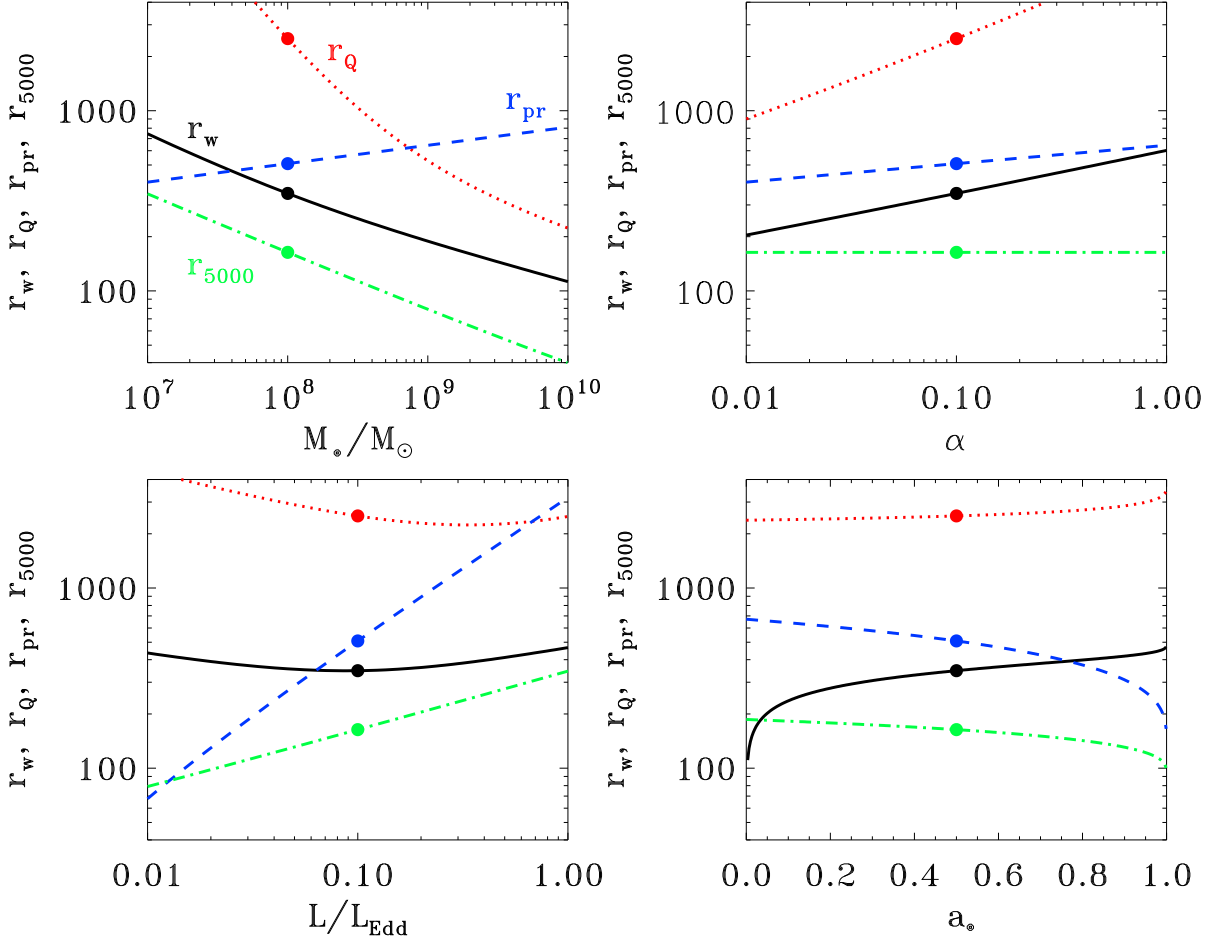


Figure 11. Characteristic disc radii versus BH mass (top left panel), Shakura–Sunyaev parameter α (top right), Eddington ratio (bottom left), and BH spin (bottom right). The curves represent the warp radius r_w (eq. 21; solid black line), radius r_Q at which the disc becomes gravitationally unstable (dotted red line), transition radius from radiation-pressure to gas-pressure dominated r_{pr} (dashed blue line) and the half-light radius at 5000 Å (dot-dashed green line). The fiducial model has $M_\bullet = 10^8 M_\odot$, $a_\bullet = 0.5$, $L/L_{\text{Edd}} = 0.1$, and $\alpha = 0.1$, and is marked by filled circles on each curve. Only a single parameter is varied away from the fiducial value to produce each panel. All radii are measured in units of the gravitational radius $R_g = GM_\bullet/c^2$.

(Peters 1964)

$$t_{\text{merge}} = \frac{5}{256} \frac{c^5 r_\star^4}{G^3 M_\bullet^3 \mu(1+\mu)}. \quad (76)$$

The numbers and orbital distribution of binary BHs are not well-constrained, either observationally or theoretically (see, for example, Shen et al. 2013). In the absence of other information, a natural place to prospect for binary BHs is where the merger time (76) is equal to the Hubble time. Thus we will use equation (76) to eliminate the unknown semimajor axis r_\star in favor of the ratio $t_{\text{merge}}/10^{10}$ yr. With this substitution and using the accretion disc models from earlier in this Section, most properties of interest are straightforward to calculate.

The binary semimajor axis is

$$r_\star = 2.0 \times 10^{17} \text{ cm} [\mu(1+\mu)]^{1/4} \left(\frac{M_\bullet}{10^8 M_\odot}\right)^{3/4} \left(\frac{t_{\text{merge}}}{10^{10} \text{ yr}}\right)^{1/4}. \quad (77)$$

The warp radius (9) is

$$r_w = 8.9 \times 10^{15} \text{ cm} \frac{(1+\mu)^{1/6}}{\mu^{1/18}} \left(\frac{a_\bullet}{0.5}\right)^{2/9} \left(\frac{M_\bullet}{10^8 M_\odot}\right)^{5/6} \left(\frac{t_{\text{merge}}}{10^{10} \text{ yr}}\right)^{1/6}. \quad (78)$$

The viscosity parameter β (eq. 30) depends on whether the warp radius is in the radiation-pressure dominated or the gas-

pressure dominated regime. In these two cases:

$$\beta_r = 0.023 \frac{\mu^{1/36}}{(1+\mu)^{1/12}} \left(\frac{0.5}{a_\bullet}\right)^{10/9} \left(\frac{L}{0.1L_{\text{Edd}}}\right)^2 \left(\frac{0.1}{\epsilon}\right)^2 \left(\frac{M_\bullet}{10^8 M_\odot}\right)^{1/12} \left(\frac{10^{10} \text{ yr}}{t_{\text{merge}}}\right)^{1/12} \frac{\mathfrak{R}_R^2}{\mathfrak{R}_T^2} \Big|_{r_w}$$

$$\beta_g = 0.079 \frac{(1+\mu)^{4/15}}{\mu^{4/45}} \left(\frac{0.5}{a_\bullet}\right)^{29/45} \left(\frac{0.1}{\alpha}\right)^{1/5} \left(\frac{L}{0.1L_{\text{Edd}}}\right)^{2/5} \left(\frac{0.1}{\epsilon}\right)^{2/5} \left(\frac{10^8 M_\odot}{M_\bullet}\right)^{7/15} \left(\frac{t_{\text{merge}}}{10^{10} \text{ yr}}\right)^{4/15} \frac{\mathfrak{R}_R^{1/5} \mathfrak{R}_T^{1/5}}{\mathfrak{R}_z} \Big|_{r_w}. \quad (79)$$

For our fiducial case – $M_\bullet = 10^8 M_\odot$, $L = 0.1L_{\text{Edd}}$, $a_\bullet = 0.5$, $\epsilon = 0.1$, $\alpha = 0.1$, $t_{\text{merge}} = 10^{10} \text{ yr}$, $\mu = 1$ – the disc becomes gas-pressure dominated at $\sim 330R_g$ (eq. 68), the warp radius is $\sim 700R_g$, the disc becomes gravitationally unstable at $2300R_g$ (eq. 70), the binary semimajor axis is $1.6 \times 10^4 R_g$, and the viscosity parameter is $\beta_g = 0.094$. For comparison, including self-gravity leads to a warp radius of $\sim 300R_g$ in an isolated disc (see discussion following eq. 72), so self-gravity is likely to have a stronger influence on the warp shape than torques from the companion BH, at least in the fiducial disc. Companion torques become stronger relative to self-gravity in binary BHs with shorter merger times t_{merge} ; of course, such systems are relatively rare because they last for less than a Hubble time.

6 SUMMARY

Warped accretion discs exhibit a remarkably rich variety of behavior. This richness arises for several reasons. First, a number of different physical mechanisms can lead to torques on the disc: the quadrupole potential from the central body (e.g., an oblate planet or a binary black hole), Lense–Thirring precession, the self-gravity of the disc, the tidal field from a companion, angular-momentum transport by viscous or other internal disc stresses, radiation pressure, and magnetic fields (we do not consider the latter two effects). Second, the geometry of the disc depends critically on whether the competing mechanisms lead to prograde or retrograde precession of the disc angular momentum around their symmetry axes. Third, a disc can support short-wavelength bending waves even when the disc mass is much smaller than the mass of the central body (as in Saturn’s rings).

Most previous studies of warped accretion discs around black holes have focused on Lense–Thirring and viscous torques (the Bardeen–Petterson approximation). If a companion star is present in the system, as in X-ray binary stars, the Bardeen–Petterson approximation is valid (a ‘high-viscosity’ disc) only if the disc viscosity is sufficiently high, $\beta\alpha_\perp \gtrsim 1$ where β is given in equation (56) for typical X-ray binary parameters and $\alpha_\perp \sim 1$ is the Shakura–Sunyaev α parameter for the internal disc stresses that damp the warp. Our results suggest that the Bardeen–Petterson approximation is not valid (a ‘low-viscosity’ disc) for quiescent X-ray binaries.

Models of such low-viscosity discs using the Pringle–Ogilvie equations of motion exhibit remarkable behavior: for a given obliquity (angle between the black-hole spin axis and companion orbital axis) there is *no* steady-state solution for β smaller than some critical value. We have argued at the end of §2.4 that the failure of these equations probably arises because they do not allow hyperbolic behavior but the question of how warped low-viscosity Lense–Thirring discs actually behave remains to be answered.

The behavior of warped accretion discs around massive black holes is equally rich. Here there is no significant companion torque (unless the black hole is a member of a binary system), but the Bardeen–Petterson approximation remains suspect because it neglects the self-gravity of the disc. In fact we find that most plausible models of AGN accretion discs have low viscosity in the sense that viscous torques are smaller at all radii than one or both of the Lense–Thirring and self-gravity torques. If the viscosity is sufficiently small, spiral bending waves are excited at the warp radius and propagate inward with growing amplitude until they are eventually damped by viscosity or non-linear effects. The presence of such waves may contribute to obscuration of the disc and the illumination of the warped disc by the central source may affect the disc spectrum or apparent size at optical wavelengths.

It is worth re-emphasizing that many of our conclusions are based on a simple model of the internal stresses in the disc – the stress tensor is that of a viscous fluid and the viscosity is related to the pressure through the Shakura–Sunyaev α parameter – that does not correspond to the actual stress tensor, which probably arises mostly from anisotropic MHD turbulence. The available evidence on the validity of this model from numerical MHD simulations, discussed at the end of §2.1, suggests that it overestimates the rate of viscous damping of warps; if correct, this would strengthen our conclusions about the limited validity of the Bardeen–Petterson approximation and the importance of tidal torques and self-gravity in shaping warped accretion discs.

Our results suggest several avenues for future work. A better treatment of self-gravitating warped discs would merge the Pringle–Ogilvie equations (28) with a description of the mutual torques due to self-gravity as in Ulubay-Siddiki et al. (2009). Generalizing the Pringle–Ogilvie equations to include wavelike behavior is also a necessary step for a complete description of warped accretion discs. Understanding the actual behavior of low-viscosity Lense–Thirring discs that exceed the critical obliquity

uity is important and challenging. Simple models of the emission from warped discs may help to resolve current discrepancies between simple flat α -disc models and observations of AGN spectra and sizes.

We thank Julian Krolik, Jerome Orosz, and Jihad Touma for illuminating discussions. We thank Gordon Ogilvie for many insights and for providing the program used to calculate the viscosity coefficients Q_i . ST thanks the Max Planck Institute for Astrophysics and the Alexander von Humboldt Foundation for hospitality and support during a portion of this work. This research was supported in part by NASA grant NNX11AF29G.

REFERENCES

- Bardeen J.M., Petterson J.A. 1975, *ApJ*, 195, L65
- Begelman M.C., Blandford R.D., Rees M.J. 1980, *Nature*, 287, 307
- Binney J. 1992, *A&ARv*, 30, 51
- Charles P., Clarkson W., Cornélisse R., Shih C. 2008, *New Astronomy Reviews*, 51, 768
- Collin-Souffrin S., Dumont A.M. 1990, *A&A*, 229, 292
- Colombo G. 1966, *AJ*, 71, 891
- Dubus G., Lasota J.-P., Hameury J.-M., Charles P. 1999, *MNRAS*, 303, 139
- Eggleton P.P. 1983, *ApJ*, 268, 368
- Fragile P.C., Mathews G.J., Wilson J.R. 2001, *ApJ*, 553, 955
- Fragile P.C., Blaes O.M., Anninos P., Salmonson J.D. 2007, *ApJ*, 668, 417
- Frank J., King A., Raine D.J. 2002, *Accretion Power in Astrophysics*. Cambridge University Press, Cambridge, UK
- Goldreich P. 1966, *Rev. Geophys. Space Phys.*, 4, 411
- Goodman J. 2003, *MNRAS*, 339, 937
- Greenhill L.J., Booth R.S., Ellingsen S.P., et al. 2003, *ApJ*, 590, 162
- Henrard J., Murigande C. 1987, *Celestial Mechanics*, 40, 345
- Herrnstein J.R., Moran J.M., Greenhill L.J., Trotter A.S. 2005, *ApJ*, 629, 719
- Hopkins P.F., Quataert E. 2010, *MNRAS*, 407, 1529
- Hopkins P.F., Hernquist L., Hayward C.C., Narayanan D. 2012, *MNRAS*, 425, 1121
- Hunter C., Toomre A. 1969, *ApJ*, 155, 747
- King A.R., Davies M.B., Ward M.J., Fabbiano G., Elvis M. 2001, *ApJ*, 552, L109
- King A.R., Pringle J.E., Livio M. 2007, *MNRAS*, 376, 1740
- Kinney A.L., Schmitt H.R., Clarke C.J., et al. 2000, *ApJ*, 537, 152
- Krolik J.H. 1999, *Active Galactic Nuclei: from the Central Black Hole to the Galactic Environment*. Princeton University Press, Princeton, NJ
- Kuo C.Y., Braatz J.A., Condon J.J., et al. 2011, *ApJ*, 727, 20
- Lai D. 1999, *ApJ*, 524, 1030
- Landau L.D., Lifshitz E.M. 2007, *The Classical Theory of Fields*, 4th ed. Butterworth Heinemann, Amsterdam
- Laplace P.S. 1805, *Traité de Méchanique Céleste*, 4. Courcier, Paris
- Lasota J.-P. 2001, *New Astronomy Reviews*, 45, 449
- Lattimer J.M., Prakash M. 2005, *Physical Review Letters*, 94, 111101
- Liu J., McClintock J.E., Narayan R., Davis S.W., Orosz J.A. 2008, *ApJ*, 679, L37 (erratum at *ApJ*, 719, L109)
- Lubow S.H., Ogilvie G.I., Pringle, J.E. 2002, *MNRAS*, 337, 706
- Maccarone T.J. 2002, *MNRAS*, 336, 1371
- Martin R.G., Pringle J.E., Tout C.A. 2009, *MNRAS*, 400, 383
- McClintock J.E., Remillard R.A. 2006, in Lewin W., van der Klis M., eds, *Compact Stellar X-ray Sources*. Cambridge University Press, Cambridge, UK, p. 157. Also arXiv:0306213.
- McClintock J.E., Narayan R., Davis S.W., et al. 2011, *Classical and Quantum Gravity*, 28, 114
- Morgan C.W., Kochanek C.S., Morgan N.D., Falco E.E. 2010, *ApJ*, 712, 1129
- Mortonson M.J., Schechter P.L., Wambsganss J. 2005, *ApJ*, 628, 594
- Murray C.D., Dermott S.F. 1999, *Solar System Dynamics*. Cambridge University Press, Cambridge, UK
- Nayakshin S. 2005, *MNRAS*, 359, 545
- Nelson R.W., Tremaine S.D. 1996, in Lahav O., Terlevich E., Terlevich R.J. eds, *Gravitational Dynamics*. Cambridge University Press, Cambridge, UK, p. 73
- Nixon C.J., King A.R. 2012, *MNRAS*, 421, 1201
- Nixon C., King A., Price D., Frank J. 2012, *ApJ*, 757, L24
- Novikov I.D., Thorne K.S. 1973, *Black Holes (Les Astres Occlus)*, 343
- Ogilvie G.I. 1999, *MNRAS*, 304, 557

- Ogilvie G.I. 2006, MNRAS, 365, 977
- Ogilvie, G.I., Latter, H.N. 2013a, MNRAS, 433, 2403
- Ogilvie, G.I., Latter, H.N. 2013b, MNRAS, 433, 2420
- Orosz J.A., McClintock J.E., Narayan R., et al. 2007, Nature, 449, 872
- Orosz J.A., Steeghs D., McClintock J.E., et al. 2009, ApJ, 697, 573
- Paczyński B. 1978, Acta Astronomica, 28, 91
- Papaloizou J.C.B., Lin D.N.C. 1995, ApJ, 438, 841
- Papaloizou J.C.B., Pringle J.E. 1983, MNRAS, 202, 1181
- Peters P.C. 1964, Physical Review, 136, 1224
- Pooley D., Blackburne J.A., Rappaport S., Schechter P.L. 2007, ApJ, 661, 19
- Pringle J.E. 1981, A&ARv, 19, 137
- Pringle J.E. 1992, MNRAS, 258, 811
- Pringle J.E. 1996, MNRAS, 281, 357
- Remillard R.A., McClintock J.E. 2006, A&ARv, 44, 49
- Scheuer P.A.G., Feiler R. 1996, MNRAS, 282, 291
- Sellwood J.A. 2013, in Oswald T.D., Gilmore G., eds, Planets, Stars and Stellar Systems Volume 5: Galactic Structure and Stellar Populations. Springer, Dordrecht, p. 923
- Shakura N.I., Sunyaev R.A. 1973, A&A, 24, 337
- Shen Y., Liu X., Loeb A., Tremaine S. 2013, arXiv:1306.4330
- Shu F.H., Cuzzi J.N., Lissauer J.J. 1983, Icarus, 53, 185
- Sorathia K.A., Krolik J.H., Hawley J.F. 2013, ApJ, 768, 133
- Sparke L.S., Casertano S. 1988, MNRAS, 234, 873
- Tanaka Y., Nandra K., Fabian A.C., et al. 1995, Nature, 375, 659
- Toomre A. 1964, ApJ, 139, 1217
- Torkelsson U., Ogilvie G.I., Brandenburg A., et al. 2000, MNRAS, 318, 47
- Tremaine S., Touma J., Namouni F. 2009, AJ, 137, 3706
- Ulubay-Siddiki A., Gerhard O., Arnaboldi M. 2009, MNRAS, 398, 535
- van Paradijs J., McClintock J.E. 1994, A&A, 290, 133
- Ward W.R. 1975, Science, 189, 377
- Yu Q. 2002, MNRAS, 331, 935
- Zhu Y., Davis S.W., Narayan R., et al. 2012, MNRAS, 424, 2504